

Z $\gtrsim 7$ GALAXIES WITH RED SPITZER/IRAC [3.6]–[4.5] COLORS IN THE FULL CANDELS DATA SET: THE BRIGHTEST-KNOWN GALAXIES AT Z ~ 7 –9 AND A PROBABLE SPECTROSCOPIC CONFIRMATION AT Z = 7.48

G. W. ROBERTS-BORSANI^{1,2}, R. J. BOUWENS¹, P. A. OESCH³, I. LABBE¹, R. SMIT^{1,4}, G. D. ILLINGWORTH⁵, P. VAN DOKKUM³, B. HOLDEN⁵, V. GONZALEZ⁶, M. STEFANON¹, B. HOLWERDA¹, S. WILKINS⁷

Draft version January 29, 2022

ABSTRACT

We identify 4 unusually bright ($H_{160,AB} < 25.5$) galaxies from HST and Spitzer CANDELS data with probable redshifts $z \sim 7$ –9. These identifications include the brightest-known galaxies to date at $z \gtrsim 7.5$. As Y-band observations are not available over the full CANDELS program to perform a standard Lyman-break selection of $z > 7$ galaxies, we employ an alternate strategy using deep Spitzer/IRAC data. We identify $z \sim 7.1$ –9.1 galaxies by selecting $z \gtrsim 6$ galaxies from the HST CANDELS data that show quite red IRAC [3.6]–[4.5] colors, indicating strong [OIII]+H β lines in the 4.5 μ m band. This selection strategy was validated using a modest sample for which we have deep Y-band coverage, and subsequently used to select the brightest $z \geq 7$ sources. Applying the IRAC criteria to all HST-selected optical-dropout galaxies over the full ~ 900 arcmin² of the CANDELS survey revealed four unusually bright $z \sim 7.1$, 7.6, 7.9 and 8.6 candidates. The median [3.6]–[4.5] color of our selected $z \sim 7.1$ –9.1 sample is consistent with rest-frame [OIII]+H β EWs of ~ 1500 Å in the [4.5] band. Keck/MOSFIRE spectroscopy has been independently reported for two of our selected sources, showing Ly α at redshifts of 7.7302 ± 0.0006 and $8.683^{+0.001}_{-0.004}$, respectively. We present similar Keck/MOSFIRE spectroscopy for a third selected galaxy with a probable 4.7σ Ly α line at $z_{\text{spec}} = 7.4770 \pm 0.0008$. All three have H_{160} -band magnitudes of ~ 25 mag and are ~ 0.5 mag more luminous ($M_{1600} \sim -22.0$) than any previously discovered $z \sim 8$ galaxy, with important implications for the UV LF. Our 3 brightest, highest redshift $z > 7$ galaxies all lie within the CANDELS EGS field, providing a dramatic illustration of the potential impact of field-to-field variance.

Subject headings: galaxies: evolution — galaxies: high-redshift

1. INTRODUCTION

The first galaxies are believed to have formed within the first 300–400 Myr of the Universe and great strides have been made towards identifying objects within this era. Since the installation of the Wide Field Camera 3 (WFC3) instrument on the Hubble Space Telescope (HST), an increasing number of candidates have been identified by means of their photometric properties, with $\gtrsim 700$ probable galaxies identified at $z \sim 7$ –8 (Bouwens et al. 2015; see also McLure et al. 2013; Schenker et al. 2013; Lorenzoni et al. 2013; Schmidt et al. 2014; Bradley et al. 2014; Mason et al. 2015; Finkelstein et al. 2014; Atek et al. 2015) and another 10–15 candidates identified even further out at $z \sim 9$ –11 (e.g., Zheng et al. 2012; Ellis et al. 2013; Oesch et al. 2014a, 2015; Bouwens et al. 2015; Zitrin et al. 2014; Zheng et al. 2014; Ishigaki et al. 2015; McLeod et al. 2015).

One of the most interesting questions to investigate

with these large samples is the build-up and evolution of galaxies. While these issues have long been explored in the context of fainter galaxies through the evolution of the UV LF, less progress has been made in the study of the most luminous galaxies due to the large volumes that must be probed to effectively quantify their evolution.

The entire enterprise of finding especially bright galaxies at $z \geq 7$ has been limited by the availability of sufficiently deep, multi-wavelength near-infrared data over wide areas of the sky. The most noteworthy such data sets are the UKIDSS UDS program (Lawrence et al. 2007), the UltraVISTA program (McCracken et al. 2012), the 902-orbit CANDELS program from the Hubble Space Telescope (Grogin et al. 2011; Koekemoer et al. 2011), the BoRG/HIPPIES pure-parallel data set (Trenti et al. 2011; Yan et al. 2011; Bradley et al. 2012; Schmidt et al. 2014; Trenti 2014), and the ZFOURGE data set (Tilvi et al. 2013; I. Labbé et al. 2016, in prep)

Of these surveys, arguably the program with the best prospects for probing the bright end of the $z > 7$ population would be the wide-area CANDELS program.⁸ The challenge with CANDELS has been that it is only covered with particularly deep near-infrared observations from 1.2 μ m to 1.6 μ m, but lacks HST-depth Y-band observations at 1.05 μ m over the majority of the

¹ Leiden Observatory, Leiden University, NL-2300 RA Leiden, Netherlands

² Department of Physics and Astronomy, University College London, Gower Street, London WC1E 6BT, UK

³ Department of Astronomy, Yale University, New Haven, CT 06520

⁴ Department of Physics and Astronomy, South Road, Durham, DH1 3EE, United Kingdom

⁵ UCO/Lick Observatory, University of California, Santa Cruz, CA 95064

⁶ University of California, Riverside, CA 92521, USA

⁷ Department of Physics & Astronomy, University of Sussex, Falmer, BRIGHTON, BN1 9QH, United Kingdom

⁸ In principle, the wide-area (~ 1 deg²) UDS and UltraVISTA programs have great potential to find large numbers of bright $z \gtrsim 6$ sources as demonstrated by the recent Bowler et al. (2014) results (see also Bowler et al. 2015), but may not yet probe deep enough to sample the $z \gtrsim 8$ galaxy population.

area. Deep observations at $1.05\mu\text{m}$ are needed for the determination of photometric redshifts for galaxies in the redshift range $z \sim 6.3$ to $z \sim 8.5$. While this can be partially compensated for by the availability of moderate-depth $1.05\mu\text{m}$ observations from various ground-based programs over the CANDELS program, e.g., HUGS (Fontana et al. 2014), UltraVISTA (McCracken et al. 2012), and ZFOURGE (I. Labbé et al. 2016, *in prep*), such observations are not available over the entire program, making it difficult to consider a search for bright $z > 7$ galaxies over the full area.

Fortunately, there appears to be one attractive, alternate means for making use of the full CANDELS area to search for bright $z > 7$ galaxies. This is to exploit the availability of uniformly deep Spitzer/IRAC observations over the full area (e.g., Ashby et al. 2013) and redshift information present in the $[3.6] - [4.5]$ colors of $z \sim 5$ – 8 galaxies. As demonstrated by many authors (e.g., Labbé et al. 2013; Smit et al. 2014, 2015; Bowler et al. 2014; Laporte et al. 2014a, 2015; Huang et al. 2016), the $[3.6] - [4.5]$ colors appear to depend on redshift in a particularly well-defined way, a dependence which appears to arise from very strong nebular emission lines, such as $H\alpha$ and $[\text{OIII}]\lambda 5007 \text{ \AA}$, which pass through the IRAC bands at particular redshifts. For example, while $z \sim 6.8$ galaxies have very blue $[3.6] - [4.5]$ colors likely due to contamination of the $[3.6]$ filter by $[\text{OIII}] + H\beta$ lines (and no similar contamination of the $[4.5]$ band), $z \geq 7$ galaxies exhibit much redder $[3.6] - [4.5]$ colors, as only the $4.5\mu\text{m}$ band is contaminated by the especially strong $[\text{OIII}] + H\beta$ lines (Labbé et al. 2013; Wilkins et al. 2013; Smit et al. 2014).

Here, we make use of the redshift information in the Spitzer/IRAC observations and apply a consistent set of selection criteria to search for bright $z \sim 8$ galaxies over all 5 CANDELS fields. A full analysis of the HST + ground-based observations is made in preselecting candidate $z \gtrsim 6$ galaxies, for further consideration with the available Spitzer/IRAC data. The identification of such bright sources allows us to better map out the bright end of the UV luminosity function (LF) at $z > 7$ and constrain quantities like the characteristic luminosity M^* or the functional form of the LF at $z > 7$. Bouwens et al. (2015) only observe a modest ($\sim 0.6 \pm 0.3$ mag) brightening in the characteristic luminosity M^* – or bright end cut-off – from $z \sim 8$ to $z \sim 5$ taking advantage of the full CANDELS + XDF + HUDF09-Ps search area ($\sim 1000 \text{ arcmin}^2$). ? also report evidence for a limited evolution in the characteristic luminosity with cosmic time, based on a wider-area search for $z \sim 6$ – 7 galaxies found over the $\sim 1.7 \text{ deg}^2$ UltraVISTA+UDS area. Limited evolution was also reported by Finkelstein et al. (2015) in subsequent work, but utilizing a ~ 3 – $15\times$ smaller area than Bouwens et al. (2015) or Bowler et al. (2015) had used.

This paper is organised as follows: §2 presents our $z \sim 5$ – 8 catalogs and data sets, as well as methodology for performing photometry. §3 describes the selection criteria we define for our samples and methodology. §4 presents the results of our investigation and discusses the constraints added by Y -band observations and Keck/MOSFIRE spectroscopy. In §5, we use the present search results to set a constraint on the bright end of

TABLE 1
SUMMARY OF DATA SETS UTILIZED IN CURRENT SEARCH.

Data Set	Area	J_{125}	Depth (5σ)		
			H_{160}	$[3.6]$	$[4.5]$
CANDELS GS DEEP	64.5	27.8	27.5	26.1	25.9
CANDELS GS WIDE	34.2	27.1	26.8	26.1	25.9
ERS	40.5	27.6	27.4	26.1	25.9
GS other ^a	31.8				
CANDELS GN DEEP	62.9	27.7	27.5	26.1	25.9
CANDELS GN WIDE	60.9	26.8	26.7	26.1	25.9
GN other ^a	34.0				
CANDELS UDS	191.2 ^b	26.6	26.8	25.5	25.3
CANDELS COSMOS	183.9 ^b	26.6	26.8	25.4	25.2
CANDELS EGS	192.4 ^b	26.6	26.9	25.5	25.3
Total	896.3				

^a Photometry over a 31.8 and 34 arcmin² area within the GS and GN fields is not available in the Bouwens et al. (2015) catalogs, due to these catalogs only including regions which have $\gtrsim 70\%$ of the full depth available in the B_{435} , V_{606} , i_{775} , z_{850} , Y_{105} , J_{125} , and H_{160} bands. For these regions, we make use of the Skelton et al. (2014) catalogs to search for $z \geq 7$ galaxies.

^b The Bouwens et al. (2015) catalogs only cover the $\sim 450 \text{ arcmin}^2$ region from the CANDELS-UDS, COSMOS, and EGS fields where deep ACS and WFC3/IR data are available from CANDELS (75% of the area). In searching the CANDELS UDS, COSMOS, and EGS fields for $z \sim 8$ candidates, we make use of the Bouwens et al. (2015) catalogs where available and the Skelton et al. (2014) catalogs otherwise.

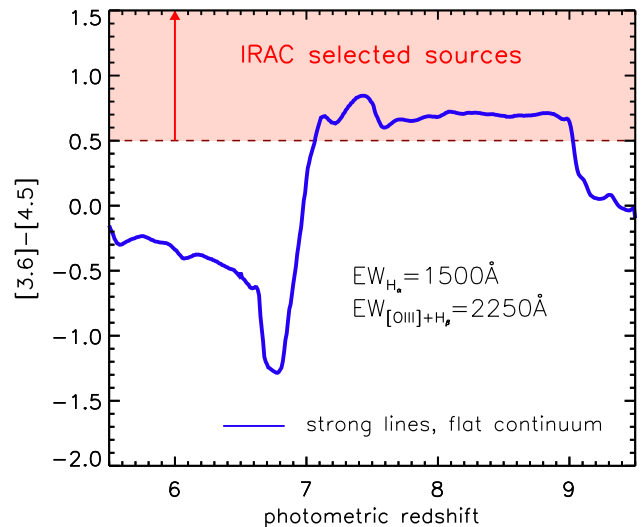


FIG. 1.— Spitzer/IRAC $[3.6] - [4.5]$ color vs. photometric redshift plot for young (~ 5 Myr) stellar population with very strong nebular emission lines ($\text{EW}_{H\alpha} = 1500 \text{ \AA}$) and a flat continuum. Also assumed are fixed flux ratios between emission lines from Table 1 of Anders & Fritze-v. Alvensleben (2003) for $0.2 Z_{\odot}$ metallicity, whilst assuming case B recombination for the $H\alpha/H\beta$ flux ratio. The $[3.6] - [4.5]$ color of galaxies is expected to become quite red at $z \gtrsim 7$ due to the impact of the $[\text{OIII}]$ line on the $4.5\mu\text{m}$ band and no comparably bright nebular line in the $3.6\mu\text{m}$.

the $z > 7$ LF. Finally, §6 includes a summary of our paper and a prospective. Throughout this paper, we refer to the HST F606W, F814W, F105W, F125W, F140W, and F160W bands as V_{606} , I_{814} , Y_{105} , J_{125} , JH_{140} and H_{160} , respectively, for simplicity. We also assume $H_0 = 70 \text{ km/s/Mpc}$, $\Omega_m = 0.3$, and $\Omega_{\Lambda} = 0.7$. All magnitudes are in the AB system (Oke & Gunn 1983).

2. OBSERVATIONAL DATA SETS, PHOTOMETRY AND $Z \sim 5-8$ SAMPLE

2.1. *HST* + ground-based data set and photometry

The sample of $z \sim 8$ galaxies we identify in this paper is based on *HST* + ground-based observations that were acquired over 5 CANDELS and ERS fields (Grogin et al. 2011; Koekemoer et al. 2011; Windhorst et al. 2011).

The near-IR *HST* observations over the CANDELS fields range in depth from ~ 4 orbits over the ~ 130 arcmin² CANDELS DEEP components in GOODS-North (GN) and GOODS-South (GS) to ~ 1 orbit depth over the ~ 550 arcmin² CANDELS WIDE component in the GN, GS, UDS, COSMOS, and EGS fields. Over the GN and GS fields, the near-IR imaging observations are available in the Y_{105} , J_{125} , and H_{160} bands, while in the UDS, COSMOS, and EGS fields, the near-IR observations are available in the J_{125} and H_{160} bands.

These fields also feature observations at optical wavelengths with the *HST* ACS camera in the B_{435} , V_{606} , i_{775} , I_{814} and z_{850} bands for CANDELS-GN+GS (with 3-10+ orbits per band), as well as V_{606} and I_{814} observations (~ 2 -orbit depth) for the CANDELS-UDS+COSMOS+EGS fields.

In addition to the *HST* observations, these fields also have very deep ground-based observations from CFHT, Subaru Suprime-Cam, VLT HAWK-I, and VISTA/VIRCAM over the latter fields. Optical data are available in CANDELS-COSMOS field in the u , g , r , i , y and z bands as part of the CFHT legacy survey, and also in the B , g , V , r , i and z bands from Subaru observations over the same field (Capak et al. 2007). The CANDELS-EGS field is observed in the same bands as the COSMOS field, as part of the CFHT legacy survey, whilst the CANDELS-UDS field is observed by Subaru as part of the Subaru XMM-Newton Deep Field (SXDF) program (Furusawa et al. 2008). For extended sources, these optical observations reach similar or greater depths to the available *HST* data over these fields (i.e., 26 mag to 28 mag at 5σ in $1.2''$ -diameter apertures: see Bouwens et al. 2015) and allow us to exclude any potential lower redshift contaminants from our samples.

Importantly, our ground-based observations also include moderately-deep (~ 26 mag at 5σ [$1.2''$ -diameter apertures]) Y -band observations which we use to constrain the nature of our selected $z > 7$ candidates (where *HST* observations are unavailable). These observations are available over the CANDELS-UDS+COSMOS fields through HAWK-I and VISTA as part of the HUGS (Fontana et al. 2014) and UltraVISTA (McCracken et al. 2012) programs, respectively. A more detailed description of the observations we utilize in constructing our source catalogs, as well as our procedure for constructing these catalogs is provided in Bouwens et al. (2015) (see Table 1, Figure 2, and §3 from Bouwens et al. 2015).

HST photometry was performed running the Source Extractor software (Bertin & Arnouts 1996) in dual-image mode, taking the detection images to be the square root of the χ^2 image (Szalay et al. 1999) and PSF-matching the observations to the H_{160} -band PSF. The colors and total magnitudes were measured with Kron-like (1980) apertures and Kron factors of 1.6 and 2.5 respectively.

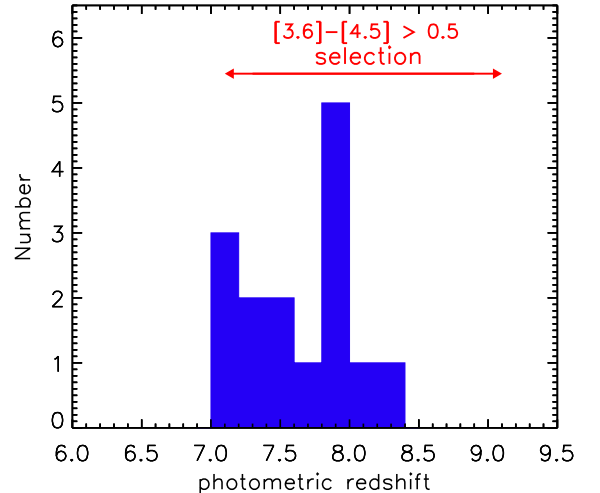


FIG. 2.— The photometric redshift distribution of the $z = 7-9$ $[3.6] - [4.5] > 0.5$ IRAC-selected control sample (including 15 sources) we used to validate our *HST*+IRAC selection technique (§3.2). The control sample of IRAC-red optical dropouts was identified exclusively from those fields with deep Y -band data (i.e., CANDELS GOODS-North, GOODS-South, UDS, COSMOS, ERS) and consider sources that are fainter than we focus on here for our primary selection (Table 2). Redshift estimates were made, based on their observed *HST* + ground-based photometry. No consideration of the Spitzer/IRAC fluxes is made in deriving the photometric redshift presented here (to ensure that the two redshift measures are entirely independent). These results strongly suggest that one can use the Spitzer/IRAC $[3.6] - [4.5]$ color to reliably distinguish $z > 7$ galaxies from $z < 7$ galaxies (especially in the present case where one makes exclusive use of those sources with relatively extreme $[3.6] - [4.5]$ colors).

Photometry on sources in the ground-based data is performed after the contamination from foreground sources is removed, using an automated cleaning procedure (Labbé et al. 2010a; Labbé et al. 2010b). The positions and two-dimensional spatial profiles of the foreground sources are assumed to match that seen in the high-spatial resolution *HST* images, after PSF-matching to the ground-based observations. The total flux in each source is then varied to obtain a good match to the light in the ground-based images. Light from the foreground sources is subsequently subtracted from the images, before doing photometry on the sources of interest. Flux measurements for individual sources are then performed in $1.2''$ -diameter circular apertures due to the objects being inherently unresolved in the ground-based observations. These flux measurements are then corrected to total, based on the model flux profiles computed for individual sources based on the observed PSFs. The procedure we employ here to derive fluxes is very similar to that employed in Skelton et al. (2014: see also Galametz et al. 2013 and Guo et al. 2013 who have also adopted a similar procedure for their ground-based photometry).

2.2. *Spitzer*/IRAC Data Set and Photometry

The detailed information we have on $z \sim 6-9$ galaxy candidates over the CANDELS fields from *HST* is nicely complemented in the mid-IR by the Spitzer Extended Deep Survey (SEDs, PI: Fazio) program (Ashby et al. 2013), which ranges in depth from 12 hours to >100 hours per pointing, though 12 hours is the typical ex-

posure time. The SEDS program provides us with flux information at $3.6\mu\text{m}$ and $4.5\mu\text{m}$, which can be useful for probing $z \sim 6-9$ galaxies in the rest-frame optical, quantifying the flux in various nebular emission lines, and estimating the redshift.

Over the GOODS-North and GOODS-South fields, we make use of Spitzer/IRAC reductions, which include essentially all the Spitzer/IRAC observations obtained to the present (Labbé et al. 2015; but see also Ashby et al. 2015), with 50-200 hours of observations per pixel in both bands (and typically ~ 100 hours).

Our procedure for performing photometry on the IRAC data is essentially identical to that used on the ground-based observations, except that we utilize $2''$ -diameter circular apertures for measuring fluxes. These fluxes are then corrected to total based on the model profile of the individual sources + the PSF. Depending on the size of the source, these corrections range from $\sim 2.2\times$ to $2.4\times$.

The median 5σ depths of these Spitzer/IRAC observations for a ~ 26 -mag source is 25.5 mag in the $3.6\mu\text{m}$ band and 25.3 mag in the $4.5\mu\text{m}$ band.

3. SAMPLE SELECTION

3.1. $[3.6]-[4.5]$ IRAC color vs. redshift and HST detections

Many recent studies (e.g., Schaerer & de Barros 2009; Shim et al. 2011; Smit et al. 2014; Labbé et al. 2013; Stark et al. 2013; de Barros et al. 2014) have presented convincing evidence to support the presence of strong nebular line contamination in photometric filters, particularly for the Spitzer/IRAC $[3.6]$ and $[4.5]$ bands. The observed $[3.6]-[4.5]$ IRAC color of galaxy candidates appear to be strongly impacted by the presence of these lines at different redshifts, in particular those of $H\alpha$ and $[\text{OIII}]$. Figure 1 provides an illustration of the expected dependence of the Spitzer/IRAC $[3.6] - [4.5]$ color, as a function of redshift, assuming an $[\text{OIII}]+\text{H}\beta$ EW (rest-frame) of $\sim 2250\text{\AA}$, which is at the high end of what has been estimated for galaxies at $z \sim 7$ (Labbé et al. 2013; Smit et al. 2014; Smit et al. 2015).

The significant change in the $[3.6] - [4.5]$ color of galaxies from $z \sim 6-7$ to $z \geq 7$ suggests this might be a promising way of segregating sources by redshift and in particular to identify galaxies at $z \geq 7$. Such information would be especially useful for search fields like CANDELS EGS, which lack deep observations in Y-band at $\sim 1.1\mu\text{m}$ to estimate the redshifts directly from the position of the Lyman break. Smit et al. (2015) have shown that selecting sources with blue $[3.6] - [4.5]$ colors can effectively single-out sources at $z \sim 6.6-6.9$ over all CANDELS fields, even in the absence of Y-band coverage.

Here we attempt to exploit this strong dependence of the $[3.6] - [4.5]$ color on redshift to identify some of the brightest $z \geq 7$ galaxies over the CANDELS fields. In performing this selection, we start with the source catalogs derived by Bouwens et al. (2015) and Skelton et al. (2014) over a $\sim 900 \text{ arcmin}^2$ region from the five CANDELS fields. In general, we will rely on the source catalogs from Bouwens et al. (2015) where they exist (covering a 750 arcmin^2 area or $\sim 83\%$ of CANDELS).⁹ Other-

wise, we will rely on the Skelton et al. (2014) catalogs and photometry.

We then apply color criterion to identify a base sample of Lyman-break galaxies at $z \sim 6.3-9.0$. In particular, over the CANDELS-UDS, COSMOS, and EGS fields, we use a

$$(I_{814} - J_{125} > 2.2) \wedge (J_{125} - H_{160} < 0.5) \wedge (I_{814} - J_{125} > 2(J_{125} - H_{160}) + 2.2) \quad (1)$$

criterion. Over the CANDELS-GN and GS fields, we require that sources satisfy one of the two color criteria defined by Eq. 2 or Eq. 3:

$$(z_{850} - Y_{105} > 0.7) \wedge (J_{125} - H_{160} < 0.45) \wedge (z_{850} - Y_{105} > 0.8(J_{125} - H_{160}) + 0.7) \wedge ((I_{814} - J_{125} > 1.0) \vee (SN(I_{814}) < 1.5)) \quad (2)$$

$$(Y_{105} - J_{125} > 0.45) \wedge (J_{125} - H_{160} < 0.5) \wedge (Y_{105} - J_{125} > 0.75(J_{125} - H_{160}) + 0.525) \quad (3)$$

These color criteria are essentially identical to those from Bouwens et al. (2015) but allow for $J_{125} - H_{160}$ colors as red as 0.5 mag to match up with the color criteria of Oesch et al. (2014) and Bouwens et al. (2015) in searching for $z > 8.5$ galaxies (i.e., $J_{125} - H_{160} > 0.5$). In so doing, it was our goal to maximize the completeness of our selection for bright $z = 7-9$ galaxies within the CANDELS program.¹⁰

These color criteria are motivated in Figure 3 of Bouwens et al. (2015) and result in a very similar redshift segregation as one achieves using photometric redshifts.

We require that sources have $[3.6] - [4.5]$ colors redder than 0.5 mag (see Figure 1). This color criterion was chosen (1) so as to require slightly redder colors than was the average color measured by Labbé et al. (2013) for their faint $z \sim 8$ sample from the HUDF (i.e., ~ 0.4) and (2) such that sources would not easily satisfy the criterion simply due to noise (requiring $> 2\sigma$ deviations for the typical source). To be certain that the IRAC colors we measured are robust, we exclude any sources where the subtracted flux from neighboring sources exceeds 65% of the original flux in a $2''$ -diameter aperture (before subtraction).

To ensure our selection is free of $z < 7$ galaxies, we required that sources show no statistically significant flux at optical wavelengths. Sources that show at least a 1.5σ detection in terms of the inverse-variance-weighted mean V_{606} and I_{814} flux with HST were excluded. In addition, we also excluded sources detected at $> 2.5\sigma$ in the deep optical imaging observations available over each field from the ground. We adopted a slightly less stringent threshold for detections in the ground-based observations, due to the impact of neighboring sources on the overall noise properties.

Finally, we consider potential contamination by low-mass stars, particularly later T and Y dwarfs (T4 and

DELS where deep optical and near-IR observations are available from the CANDELS observations.

¹⁰ We remark that any contaminants in a particularly bright selection would be generally easy to identify given the depth of the HST, Spitzer, and supporting ground-based observations.

⁹ Bouwens et al. (2015) only considered those regions in CAN-

later), where the $[3.6] - [4.5]$ color can become quite a bit redder than 0.5 mag (Kirkpatrick et al. 2011; Wilkins et al. 2014). To exclude such sources from our samples, both the spatial information we had on each source from the SExtractor stellarity parameter and total SED information were considered. Sources with measured stellarities > 0.9 were identified as probable stars (where 0 and 1 corresponds to extended and point-like sources, respectively), as were sources with measured stellarity parameters > 0.5 if the flux information we had available for sources was significantly better fit ($\Delta\chi^2 > 2$) with a low-mass stellar model from the SpecX prism library (Burgasser et al. 2004) than with the best-fit galaxy SED model, as derived by the Easy and Accurate Zphot from Yale (EAZY; Brammer et al. 2008) software. Our SED fits with EAZY considered both the standard SED templates from EAZY and SED templates from the Galaxy Evolutionary Synthesis Models (GALEV; Kotulla et al. 2009). Nebular emission lines, as described by Anders & Fritze-v. Alvensleben (2003), were added to the GALEV SED template models assuming a $0.2Z_{\odot}$ metallicity.

No sources were removed from our selection as probable low-mass stars. The procedure we use here to exclude low-mass stars from our selection is identical to that utilized by Bouwens et al. (2015).

3.2. Validation of Selection Technique

Before applying the selection criteria from §3.1 to the $\sim 900\text{-arcmin}^2$ CANDELS + ERS search fields, it is useful to first test these criteria on those data sets which feature deep z and Y -band observations. The availability of observations at these wavelengths, together with observations at both redder and bluer wavelengths with HST, allows for very accurate estimates of the redshifts for individual sources. There are five data sets that possess these observations: (1) CANDELS GOODS-S, (2) CANDELS GOODS-N, (3) ERS, (4) CANDELS UDS, and (5) CANDELS COSMOS field. The first three feature these observations with HST and the latter two using ground-based telescopes.

We apply selection criteria from the previous section to a H_{160} -band limiting magnitude of 26.7 mag for the first three fields and 26.5 mag for the latter two. Our decision to use these depths is partially guided by the sensitivity of the Spitzer/IRAC data over these fields.

Applying the selection criteria from the previous section to the CANDELS GN+GS and ERS fields ($H_{160,AB} < 26.7$), we find 7 sources that satisfy our selection criteria. For each of these sources, we estimate photometric redshifts with EAZY. In fitting to the observed photometry, we used the same standard EAZY SED templates as we described in the previous section.

We also applied the above selection criteria to the CANDELS-UDS and CANDELS-COSMOS fields, where it is also possible to estimate photometric redshifts, making use of the available HST observations and ground-based optical and near-IR Y and K band observations. Eight sources satisfy these criteria.

All 15 of the sources selected using the criteria from the previous section are presented in Figure 2 and fall between $z = 7.0$ and $z = 8.3$, which is the expected range if a high-EW [OIII]+H β line is responsible for red $[3.6] - [4.5]$ colors in these galaxies. This suggests that

the criteria we propose in the previous section can be effective in identifying a fraction of $z \geq 7$ galaxies that are present in fields with deep HST+Spitzer observations. The individual coordinates, colors, and estimated redshifts for individual sources from this validation sample can be found in Table 5 located in Appendix B.

In recommending the use of the IRAC photometry to subdivide $z \sim 6\text{--}9$ samples by redshift, we should emphasize that the most robust results will be obtained making use of only those sources with the smallest confusion corrections. While we took care in the selection of both our primary sample (and the sample we used to validate the technique) to avoid such sources, such sources were not excluded in making Figure 1 of Smit et al. (2015: resulting in a few $z > 7$ sources with anomalously blue Spitzer/IRAC colors). Despite this issue with Smit et al. (2015) Figure 1, we emphasize that this is nevertheless not a major concern for sources in their $z = 6.6\text{--}6.9$ sample. Only 2 of the 15 sources in the latter sample were subject to a $\sim 3\times$ correction for flux from neighboring sources and those 2 sources (GSD-2504846559 and EGS-1350184593) are flagged as less reliable.

3.3. Search Results for Bright $H_{160,AB} < 25.5$ Galaxies

Here we focus on the identification of only the brightest $H_{160,AB} < 25.5$ $z \geq 7$ galaxies using our Spitzer/IRAC color criteria. This is to keep the current selection small and to focus on sources whose surface density was particularly poorly defined from previous work. Prior to this work, the only study which identified such bright $z \sim 8$ sources was Bouwens et al. (2015). Focusing on the brightest sources is also valuable, since it allows us to obtain very precise constraints on SED shapes and its Spitzer/IRAC colors of the sources, as well as providing opportunities for follow-up spectroscopy (see §4.2).

Applying the selection criteria described in §3.1 on the CANDELS-GS, CANDELS-GN, CANDELS-UDS, CANDELS-COSMOS and CANDELS-EGS fields, we identify a total of 4 especially bright ($H_{160,AB} < 25.5$) candidate $z \geq 7$ galaxies.

Our 4 candidate $z \geq 7$ galaxies are presented in Table 2 and in Figure 3. We see from Figure 3 that each candidate is clearly visible in the HST H_{160} and J_{125} filters, as well as the IRAC 3.6 μm and 4.5 μm bands. Of course, no significant detection is evident in the HST V_{606} and I_{814} bands for these sources. This would suggest that these sources show a break in their spectrum somewhere between 0.9 μm and 1.2 μm and therefore have redshifts between $z \sim 6$ and $z \sim 8.5$. [We discuss the impact of information from Y -band observations available over 3 of the 4 candidates in §4.1.]

3 of these 4 bright sources are found in the CANDELS-EGS field. Sources from this field were not included in our earlier attempt to validate the present selection technique (§3.2), so only one of these new sources is in common with the 15 sources just discussed.

To derive constraints on the redshift of each bright source, we again made use of EAZY. The photometry provided to EAZY included fluxes from HST filters, IRAC 3.6 μm and 4.5 μm filters and ground based telescopes. Using EAZY allows us to generate a best-fit SED of each galaxy candidate as well as its redshift likelihood distribution ($P(z)$), which we present in Figure 4, with the observed galaxy flux points overplotted. From the

TABLE 2
A COMPLETE LIST OF THE RESULTING $z \geq 7$ SOURCES IDENTIFIED AFTER APPLYING OUR SELECTION CRITERIA.

ID	R.A.	Dec	m_{AB}^a	[3.6]–[4.5]	z_{phot}^b	$Y_{105} - J_{125}^c$	References*
COSY-0237620370	10:00:23.76	02:20:37.00	25.06 ± 0.06	1.03 ± 0.15	$7.14^{+0.12}_{-0.12}$	-0.13 ± 0.66	[1],[2],[3]
EGS-zs8-1	14:20:34.89	53:00:15.35	25.03 ± 0.05	0.53 ± 0.09	$7.92^{+0.36}_{-0.36}$	1.00 ± 0.60	[3], [4]
EGS-zs8-2	14:20:12.09	53:00:26.97	25.12 ± 0.05	0.96 ± 0.17	$7.61^{+0.26}_{-0.26}$	0.66 ± 0.37	[3]
EGSY-2008532660	14:20:08.50	52:53:26.60	25.26 ± 0.09	0.76 ± 0.14	$8.57^{+0.22}_{-0.43}$		

* References: [1] Tilvi et al. 2013, [2] Bowler et al. 2014, [3] Bouwens et al. 2015, [4] Oesch et al. 2015b

^a The apparent magnitude of each source in the H_{160} band.

^b The photometric redshift estimated by EAZY, including flux measurements in the Y band. The uncertainties quoted here correspond to 1σ .

^c The $Y - J$ color for each source. The COSMOS candidate uses ground based data whilst the EGS candidates use Y_{105} and J_{125} filters (where available).

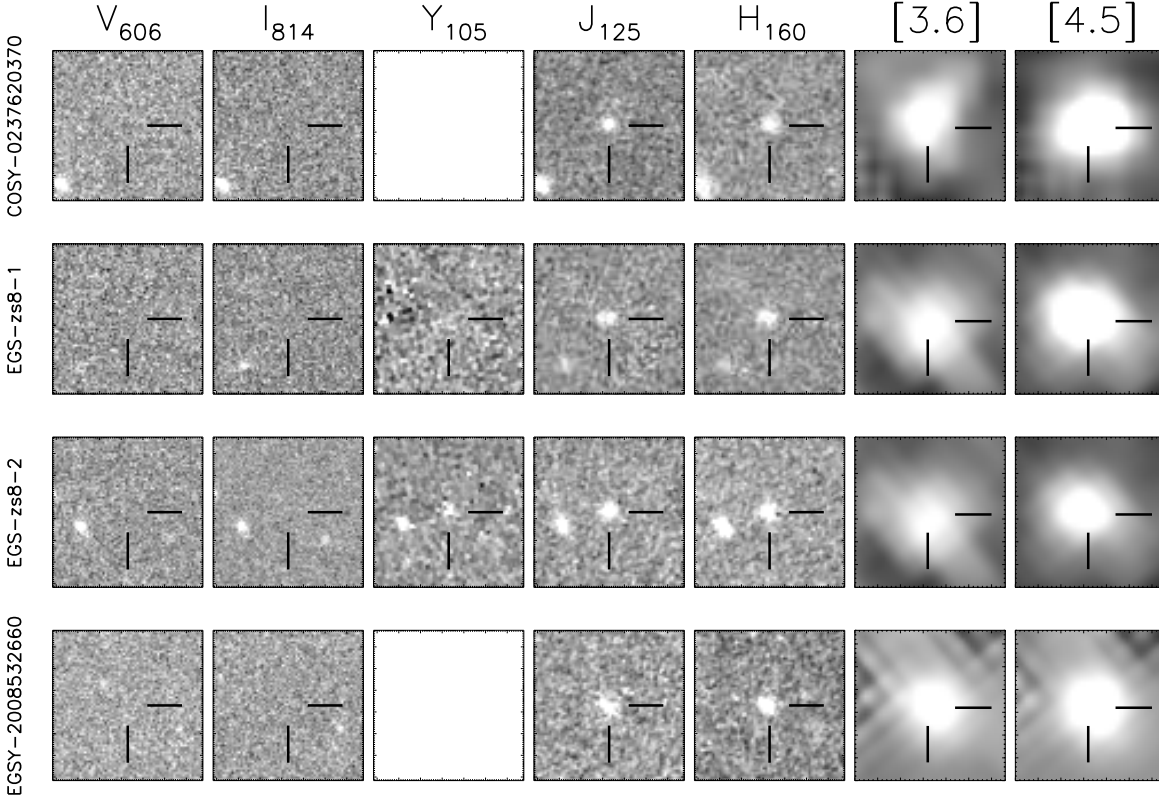


FIG. 3.— HST/ACS $V_{606} I_{814}$, HST/WFC3 $Y_{105} J_{125} H_{160}$, and Spitzer/IRAC $3.6\mu m + 4.5\mu m$ postage stamp images ($4'' \times 4''$) of the 3 $z \geq 7$ candidates identified over the 5 CANDELS fields. On the Spitzer/IRAC images, flux from neighbouring sources has been removed. Y -band observations at $1.05\mu m$ are also available for COSY-0237620370 from ground-based programs (ZFOURGE [Tilvi et al. 2013], UltraVISTA [Bowler et al. 2014]).

SED plots, we observe a near-flat rest-frame optical continuum, as well as emission lines dominating at the location of high flux points, highlighting the contribution of strong nebular emission lines to the instrument filters.

One of our $z \geq 7$ candidates, i.e., EGS-zs8-2, is sufficiently compact, as can be seen from Figure 3, that we considered the possibility that it may correspond to a star. To test this possibility, we compare its SED to all the stellar SEDs in the SpecX prism library and find the best-fitting stellar SED. The χ^2 goodness-of-fit for the stellar SED is an order of magnitude greater than the galaxy SED. In addition, the SExtractor stellarity we measure for EGS-zs8-2 in the J_{125} and H_{160} bands is 0.60 and 0.33 (where 0 and 1 correspond to an extended and point source, respectively), which significantly favors EGS-zs8-2 corresponding an extended source. Bouwens

et al. (2015) ran an extensive number of end-to-end simulations to test the possibility that point-like sources could scatter to such low measured stellarities. Stellarities of ~ 0.60 are only found for $H_{160,AB} \sim 25$ -mag point-like sources in $<2\%$ of the simulations that Bouwens et al. (2015) run. Therefore, both because of the spatial and spectral information, we can be confident that the EGS-zs8-2 candidate is a $z \geq 7$ galaxy and not a low-mass star. However, as we show in §4.2, perhaps the most convincing piece of evidence for this source corresponding to a $z > 7$ galaxy is our discovery of a plausible 4.7σ Ly α line in the spectrum of this source at $1.031\mu m$ (Figure 8).

A second candidate from our selection, COSY-0237620370, is also very compact and could potentially also correspond to a low-mass star. However, like EGS-zs8-2, the photometry of the source is bet-

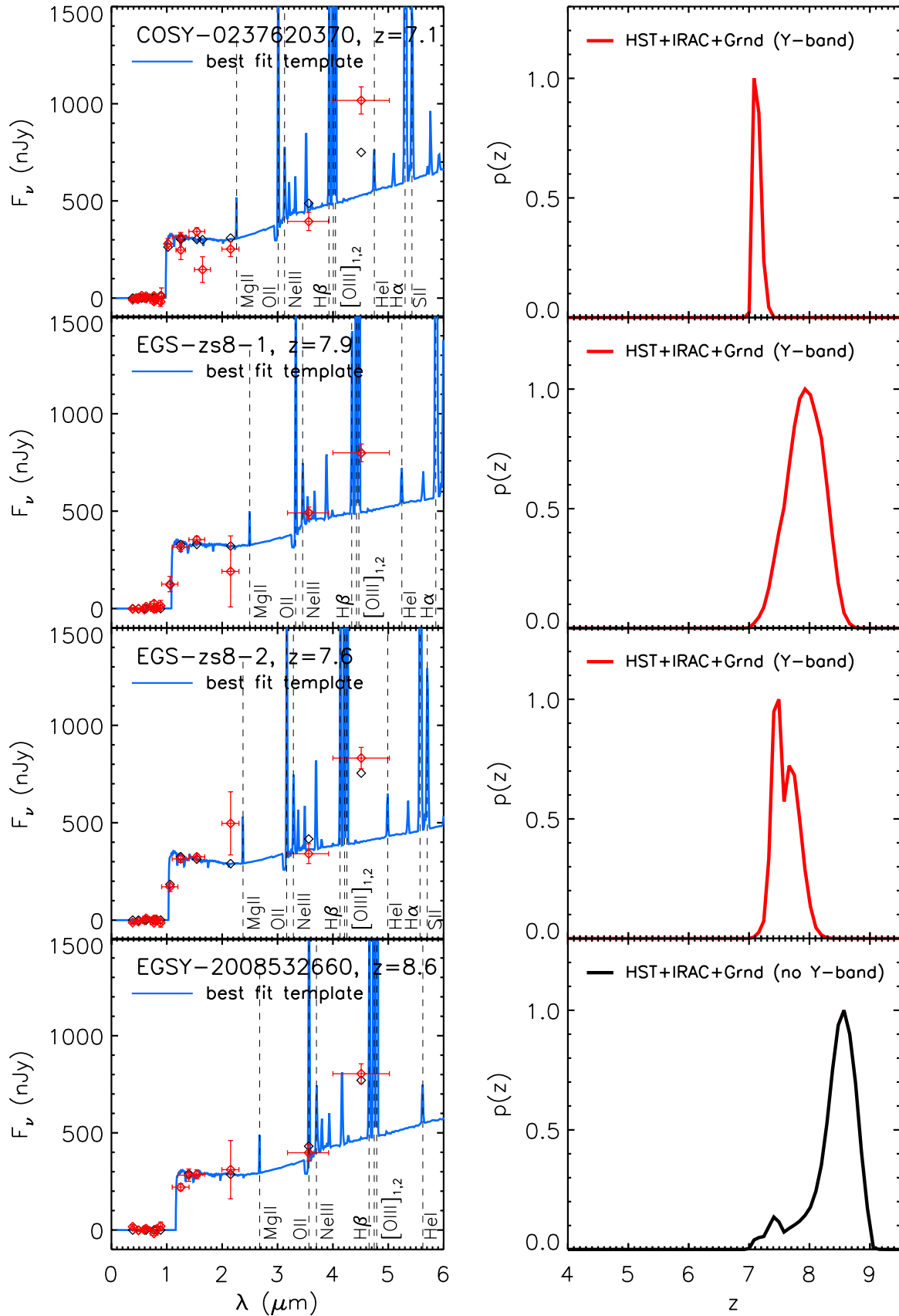


FIG. 4.— *Left*: Best-fit SED models (*blue line*) to the observed HST + Spitzer/IRAC + ground-based photometry (*red points and error bars*) for the 4 especially bright ($H_{160,AB} < 25.5$) $z \geq 7$ galaxies selected using our IRAC-red selection criteria ($[3.6] - [4.5] > 0.5$). Also included on the figure is the redshift estimate for the best-fit model SED provided by EAZY. *Right*: Redshift likelihood distributions $P(z)$ for the same 4 candidate $z \geq 7$ galaxies, as derived by EAZY. The impact of the Spitzer/IRAC photometry on the redshift likelihood distributions should be close.

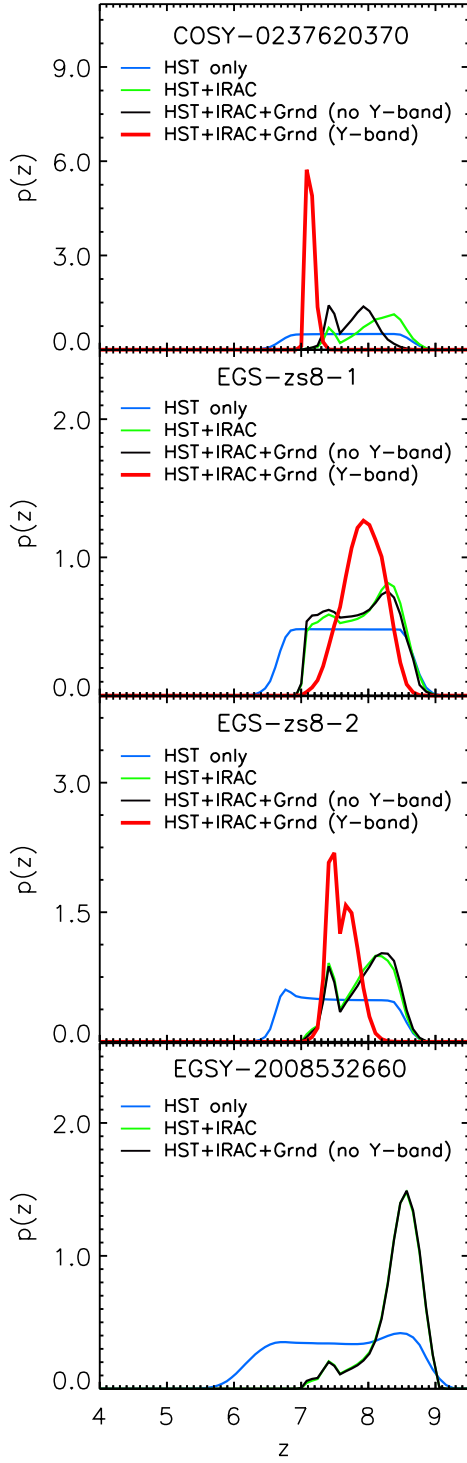


FIG. 5.— Redshift likelihood $P(z)$ constraints for the respective galaxy candidates presented in Figure 4 shown considering the impact of various subsets of the photometry (i.e., HST only, HST+IRAC, HST+IRAC+ground-based observations (no Y-band and Y-band included)). It is clear that the addition of both the Spitzer/IRAC observations and the Y-band observations result in a much tighter distribution and allows for a much more accurate estimation of the photometric redshift.

ter fit with a galaxy SED than a stellar SED (with a $\chi^2(\text{star}) - \chi^2(\text{galaxy}) = 17.2$) and the source shows evidence for spatial extension, with a measured stellarity of 0.81 and 0.34 in the J_{125} and H_{160} bands, respectively. Stellarities even as high as 0.81 are only recovered in $\sim 5\%$ of the end-to-end simulations Bouwens et al. (2015) run at $H_{160,AB}$ -band magnitudes of ~ 25.0 . Earlier, Tilvi et al. (2013) obtained the same conclusion regarding this candidate from the ZFOURGE program, where consistent fluxes are found in the near-infrared medium bands strongly arguing against this source corresponding to a low-mass star. Bowler et al. (2014) also conclude this source is extended and not a low-mass star, based on its spatial profile (see Figure 6 from Bowler et al. 2014) and based on its observed photometry where $\chi^2(\text{star}) - \chi^2(\text{galaxy}) = 13.0$.

Flux information from HST, Spitzer/IRAC, and ground-based observations all have value in constraining the redshifts of the candidate $z \geq 7$ galaxies we have identified in the present probe. While the HST flux information we have available for all three candidates in the $V_{606}I_{814}J_{125}JH_{140}H_{160}$ bands only allow us to place them in the redshift interval $z \sim 6.5-9.0$ (blue line in Figure 5), we can obtain improved constraints on the redshifts of the candidates incorporating the flux information from Spitzer/IRAC and from deep ground-based observations. Each of these three candidates appears to have redshifts robustly between $z \sim 7.0$ and $z \sim 8.6$ (red and black lines in Figure 5). In addition, as we discuss in §4.1 and show in Figure 5, the availability of the Y/Y₁₀₅-band observations allows us to significantly improve our redshift constraints on all three candidates.

We used the Bouwens et al. (2015) catalogs to search 83% of the total area of the CANDELS fields and the Skelton et al. (2014) photometric catalogs otherwise (in those regions over the WFC3/IR CANDELS fields which lack the deep HST/ACS data). As a check on the search results we obtained with the Bouwens et al. (2015) catalogs, we applied the same selection criteria to the Skelton et al. (2014) catalogs. Encouragingly, we identified 75% of our sample, with only one candidate missing due to its having a $[3.6] - [4.5]$ color of 0.47 mag. For all 4 candidates from our primary sample, we find that our derived $[3.6] - [4.5]$ colors are almost identical to those quoted by Skelton et al. (2014), agreeing to ≤ 0.1 mag (and typically $\Delta[3.6] - [4.5]$ of 0.05 mag).

We also identified 1 additional bright ($H_{160,AB} < 25.5$) $z \geq 7$ candidate in the CANDELS-EGS field not identified in our primary search (see Appendix A). It seems clear examining its photometry that this source is extremely likely to be at $z \sim 7-9$ (and indeed it appears in the Bouwens et al. 2015 $z \sim 8$ sample). However, since its measured $[3.6] - [4.5]$ color is 0.22 ± 0.06 mag in our photometric catalog (0.3 mag bluer than in the Skelton et al. 2014 catalog), we did not include it in our primary sample. We remark that photometry for this source was more challenging due to its being located close to a bright neighbor and its being a two-component source.

3.4. Possible Evidence for Lensing Amplification of Selected $z > 7$ Sources

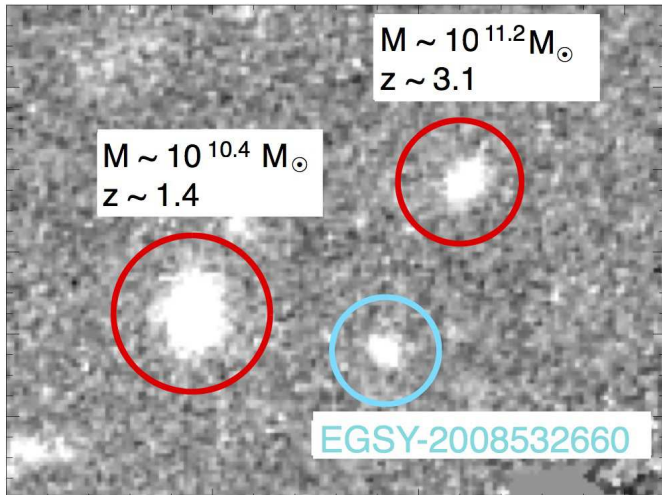


FIG. 6.— Image of the area ($9.6'' \times 7.2''$) surrounding our new $z \sim 8.6$ candidate EGSY-2008532660. EGSY-2008532660 lies very close ($< 3''$) to two bright, apparently massive foreground galaxies (§3.4). Based on the position of the foreground sources and their inferred masses, we estimate that EGSY-2008532660 is likely magnified by a modest factor, i.e., $\sim 1.8\times$.

For very high redshift sources ($z \gg 6$), it is expected that the sources with the brightest apparent magnitudes will benefit from gravitational lensing (Wyithe et al. 2011; Barone-Nugent et al. 2015; Mason et al. 2015; Fialkov & Loeb 2015), and indeed it is found that a small fraction of the brightest galaxies identified over the CANDELS program are consistent with being boosted by gravitational lensing (Barone-Nugent et al. 2015).

To investigate whether any of the bright $z \geq 7$ galaxies identified in our search might be gravitationally lensed, we considered all sources within $5''$ of our candidates in the Skelton et al. (2014) catalogs and used the estimated redshifts, stellar masses, and sizes from these catalogs to derive Einstein radii for the foreground sources assuming a single isothermal sphere model. We then calculated the degree to which our bright $z \geq 7$ galaxy candidates might be magnified by the foreground sources.

In only one case was the expected magnification level $> 10\%$ and this was for our $z \sim 8.6$ candidate EGSY-2008532660. In this case, we identified two foreground galaxies which could significantly magnify this candidate (Figure 6). The first was a $10^{10.4} M_\odot$ mass, $z \sim 1.4$ galaxy (14:20:08.81, 52:53:27.2) with a separation of $2.8''$ from our $z \sim 8.6$ candidate. The second was a $10^{11.2} M_\odot$ mass, $z \sim 3.1$ galaxy (14:20:08.37, 52:53:29.1) with a separation of $2.7''$ from our $z \sim 8.6$ candidate. Using the measured size of the two sources, we derive $\sigma \sim 170$ km/s and $\sigma \sim 370$ km/s for the velocity dispersion. We checked and these velocity dispersions are fairly similar to what fitting formula in Mason et al. (2015) yield (i.e., using the relation in their Table 1 and applying H_{160} -band or IRAC $3.6\mu\text{m}$ apparent magnitudes depending on whether we are considering the $z \sim 1.4$ or $z \sim 3.1$ source).

Based on the observed separation of this source from our $z \sim 8.6$ galaxy, we estimate a lensing magnification of 20% and a factor of 1.8 from the former and latter foreground sources. In computing these magnification factors, we assume that the mass profile of galaxies is an isothermal sphere and taking the magnification factor to

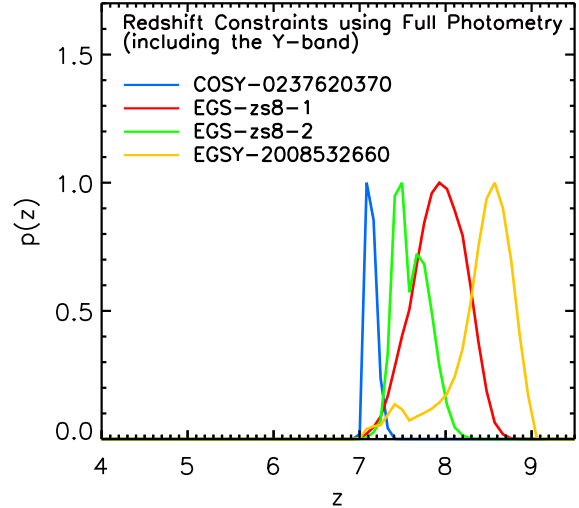


FIG. 7.— Redshift likelihood distributions $P(z)$ for the 4 $H_{160,AB} < 25.5$ sources in our $z \geq 6$, IRAC ultra-red selection. These likelihood distributions include flux constraints from the ground-based and HST Y-band observations. Our three highest redshift sources have $z_{\text{phot}} = 7.6 \pm 0.3$, $z_{\text{phot}} = 7.9 \pm 0.4$, and $z_{\text{phot}} = 8.6^{+0.2}_{-0.4}$.

be $1/(1 - \theta_E/\theta)$ where θ is separation from the neighboring sources and θ_E is the Einstein radius. Looking at the morphology of EGSY-2008532660, we see no clear evidence to suggest that the galaxy is highly magnified and there is no obvious counterimage. However, we clearly cannot rule out smaller lensing amplification factors, particularly if the intrinsic size of the source is small. As the inferred stellar or halo masses for the neighboring galaxies is not precisely known, this translates into a modest uncertainty into the actual luminosity of this source (as much as 0.3 dex). Given this fact, we consider it safest for us to exclude it from analyses of the UV LF.

4. VALIDATION OF OUR $Z \sim 8$ SELECTION

Here we attempt to determine the nature of the $z > 7$ candidates we selected using the HST+Spitzer/IRAC+ground-based observations using some Y-band observations that became available over a few of our candidates and using the results of some follow-up spectroscopy that we performed (first reported in Oesch et al. 2015b).

4.1. Y-band Photometric Observations

Deep observations at $1.05\mu\text{m}$ are particularly useful in ascertaining the nature of these candidates and also their redshift, due to the Y-band photometry providing constraints on the position of the Lyman break as it redshifts from $1.2\mu\text{m}$ to $0.9\mu\text{m}$.

Deep observations at $1.05\mu\text{m}$ are available for 3 of the 4 $z \geq 7$ candidates that we selected as part of our $H_{160,AB} < 25.5$ sample. Y-band observations of the COSY-0237620370 candidate are available from the 3-year UltraVISTA observations (McCracken et al. 2012), while HST Y_{105} -band observations are available over 2 other candidates in our selection as a result of some recent observations from the z9-CANDELS follow-up pro-

gram (Bouwens 2014; Bouwens et al. 2016).¹¹

We make these estimates in an identical way to what we did previously. Our redshift constraints, including the Y-band, are presented in Table 2. Furthermore, we present the HST Y_{105} filter images in Figure 3, where we observe a clear detection in the Y_{105} filters for EGS-zs8-1 and EGS-zs8-2 and no detection in the V_{606} or I_{814} filters, indicating a $z \sim 7$ Lyman dropout. For EGS-zs8-1, however, we observe little to no detection in the Y_{105} filter but a clear detection in the J_{125} filter which indicates this galaxy is observed at $z \sim 8$.

Figure 4 and 7 presents the redshift likelihood distributions on our $z \geq 7$ candidates, incorporating the Y-band observations from UltraVISTA and HST. It is evident from Figure 5 that the Y-band data greatly improves our constraints on the redshift of the individual candidates in our selection. Together with the results in §3.2 and Figure 2, these results largely validate our selection technique.

4.2. Keck/MOSFIRE Spectroscopic Follow-up

4.2.1. Observations and Reduction

In addition to using photometric data in the Y-band to validate our method, we also tested this method by obtaining deep near-IR spectroscopy on 2 sources from the current selection. Oesch et al. (2015b) already provided a first description of the observational set-up we utilized for half of our targets, so we keep the current discussion short. A total of 4 hours of good Y-band spectroscopy were obtained in the CANDELS-EGS field with the Multi-Object Spectrometer for Infra-Red Exploration (MOSFIRE: McLean et al. 2012) instrument on the Keck I telescope. Two masks (see Fig. 2 of Oesch et al. 2015) were utilized and our spectra were taken with 180 s exposures at a spectral resolution of $R=3500$ and $R=2850$ (for a $0.7''$ and $0.9''$ slit respectively) over 3 nights (April 18, April 23, April 25, 2014 - although due to poor weather conditions, April 18 was effectively lost), with the aim of searching for Ly α emission in EGS-zs8-1 and EGS-zs8-2. Each mask contains a slitlet placed on a star, which we use for monitoring the sky transparency and observing conditions of each exposure. These observations were reduced using a modified version of the DRP MOSFIRE reduction code pipeline (for details see Oesch et al. 2015b). The spectra complement the photometric data sets for these two galaxies and allow us to confirm their redshifts.

4.2.2. Ly α Emission Lines

The observations carried out with Keck/MOSFIRE revealed candidate Ly α emission lines in the spectra of both EGS-zs8-1 and EGS-zs8-2. The detection of a Ly α line for EGS-zs8-1 appears to be robust (a 6.1σ detection with a line flux of $f_{Ly\alpha} = 1.7 \pm 0.3 \times 10^{-17}$ erg s $^{-1}$) and places that source at $z_{Ly\alpha} = 7.7302 \pm 0.0006$, as first reported by Oesch et al. (2015b).¹²

¹¹ The purpose of the z9-CANDELS program was to determine the nature of high-probability but uncertain candidate $z \sim 9$ -10 galaxies over the CANDELS-UDS, COSMOS, and EGS fields. In some cases, bright candidate $z \sim 8$ galaxies were located nearby bright $z \sim 9$ -10 candidates and could be readily observed in the same pointings.

¹² The flux uncertainties that we derive for this candidate and EGS-zs8-2 is almost an order-of-magnitude larger than found in ob-

The 1D and 2D spectra for our other targeted $z > 7$ candidate EGS-zs8-2 is presented in Figure 8 (see also Figure 2 in Oesch et al. 2015b for spectra of the confirmed $z = 7.7302 \pm 0.0006$ candidate). Using a simple gaussian to determine the central wavelength of the observed line at $1.031\mu\text{m}$ (and ignoring asymmetry and other effects due to skylines surrounding this candidate Ly α line), we determine the spectroscopic redshift for the source to be $z_{Ly\alpha} = 7.4770 \pm 0.0008$, with a detection significance of 4.7σ for the line and a line flux of $f_{Ly\alpha} = 1.6 \pm 0.3 \times 10^{-17}$ erg s $^{-1}$ cm $^{-2}$. While this line is only detected at 4.7σ significance, its reality appears to be supported by subsequent near-infrared spectroscopy obtained on this source from independent observing efforts (D. Stark et al. 2016, in prep).

In addition to the Ly α -emission lines reported by Oesch et al. (2015b) and this work, Zitrin et al. (2015) report the detection of a 7.5σ Ly α line for our EGSY-2008532660 candidate in new Keck/MOSFIRE observations (June 10-11, 2015). This redshift measurement sets a new high-redshift distance record for galaxies with spectroscopic confirmation. Our photometric selection therefore contains 3 of the 4 most distant, spectroscopically-confirmed galaxies to date.

The $z_{Ly\alpha} = 7.730$, $z_{Ly\alpha} = 7.477$ and $z_{Ly\alpha} = 8.683$ redshifts for EGS-zs8-1, EGS-zs8-2 and EGSY-2008532660, respectively, are in excellent agreement with the photometric redshifts derived for these galaxies using HST+IRAC+Ground based observations and our color criteria. The absolute magnitude and redshifts of EGS-zs8-1, EGS-zs8-2, and EGSY-2008532660 are presented in the top panel of Figure 9 in relation to other $z > 6.5$ galaxies with clear redshift determinations from Ly α .

The current spectroscopy provides us with considerable reassurance that our proposed color technique is an effective method to search for bright, $z \geq 7$ galaxies.¹³

5. COMPARISON WITH PREVIOUS WORK

Three of our four candidates were already identified as part of previous work. Tilvi et al. (2013) identified COSY-0237620370 as a $z \sim 7$ galaxy by applying Lyman-break-like criteria to the deep medium-band ZFOURGE data and estimate a redshift of $7.16^{+0.35}_{-0.19}$. This source was also identified by Bowler et al. (2014) as a $z \sim 7$ galaxy (211127 in the Bowler et al. 2014 catalog) using the deep near-IR observations from the Ultra-VISTA program and derived a photometric redshift of $7.03^{+0.12}_{-0.11}$ for the source (or 7.20 if the source exhibits prominent Ly α emission), similar to what we find here. Tilvi et al. (2013) derive

observations of similar $z > 7$ (e.g., Finkelstein et al. 2013). This is in part due to the significantly poorer seeing conditions we were subject for the observations ($1.00''$ FWHM instead $0.65''$ for Finkelstein et al. 2013). Another potentially significant contributing factor is our relatively conservative account of the uncertainties in the line flux measurements, including uncertainties that arise from the sky subtraction. The uncertainties we derive are consistent with typical values reported by the MOSDEF program (Kriek et al. 2015).

¹³ Interestingly enough, D. Stark et al. (2016, in prep) have also spectroscopically confirmed that the fourth source (COSY-0237620370) from our sample lies at $z=7.15$. As such, Ly α emission has been found in all 4 galaxies that make up our selection. Our entire sample has therefore been spectroscopically confirmed to lie in the redshift range $z = 7.1$ -9.1, with the spectroscopic redshifts being in excellent agreement with our derived photometric redshifts.

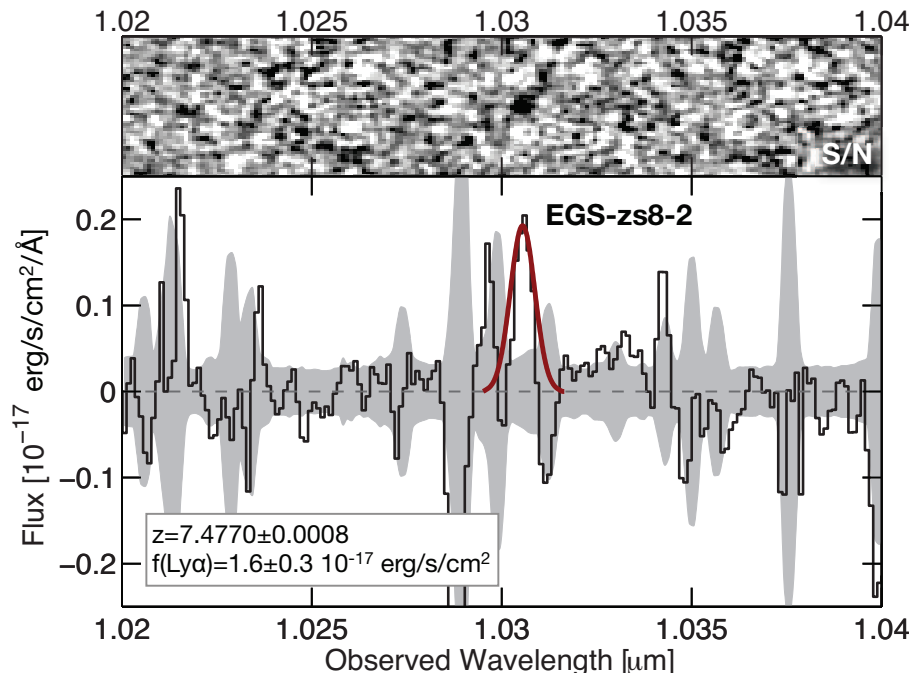


FIG. 8.— Keck/MOSFIRE spectra of EGS-zs8-2. The 2D spectrum after a 2×2 binning is presented in the upper panel, while the extracted 1D spectrum is shown in the lower panel. The gray shaded area represents the 1σ flux uncertainty, the red line shows the best-fit Gaussian. A candidate $\text{Ly}\alpha$ line (detected at 4.7σ significance) is apparent at $1.031\mu\text{m}$ between two sky lines. Using a simple gaussian to model the shape and position of this line suggests a redshift of $z = 7.4770 \pm 0.0008$ for this source (see also D. Stark et al. 2016, in prep). The other $z > 7$ candidate here targeted with spectroscopy also shows a prominent $\text{Ly}\alpha$ line, with a measured redshift of 7.7302 ± 0.0006 (Oesch et al. 2015b).

a $[3.6] - [4.5]$ color of 1.96 ± 0.54 mag, while Bowler et al. (2014) find 0.7 ± 0.3 mag, both of which are broadly consistent with what we find here.

Bouwens et al. (2015) identified 3 of the 4 sources as part of their search for $z \sim 7-8$ galaxies over the five CANDELS fields and segregated the sources into different redshift bins using the photometric redshift estimates. The full HST + Subaru Suprime-Cam $BgVriz$ + CFHT Megacam $ugriyz$ + UltraVISTA $YJHK_s$ photometry was used to estimate these redshifts for the candidate in the COSMOS field. Meanwhile, the HST + CFHT Megacam $ugriyz$ + WIRCam K_s + Spitzer/IRAC $3.6\mu\text{m}4.5\mu\text{m}$ photometry was used in the case of the two EGS candidates.

Bouwens et al. (2015) derived a photometric redshift of $z = 7.00$ for COSY-0237620370 over the CANDELS-COSMOS field and derived photometric redshifts of 8.1 for the two sources over the CANDELS-EGS field (EGS-zs8-1 and EGS-zs8-2, respectively), so the latter two candidates were placed in the $z \sim 8$ sample of Bouwens et al. (2015).

There was, however, some uncertainty as to both the robustness and also the precise redshifts of the CANDELS-EGS candidates from Bouwens et al. (2015). Prior to the present study, the use of the $[3.6] - [4.5]$ color has never been systematically demonstrated to work for the identification of galaxies with redshifts of $z > 7$ despite there being ~ 5 prominent examples of $z \geq 7$ galaxies with particularly red $[3.6] - [4.5]$ colors (Bradley et al. 2008; Ono et al. 2012; Finkelstein et al. 2013; Tilvi et al. 2013; Laporte et al. 2014, 2015). Moreover, no Y_{105} -band observations were available over either $z \geq 7$ candidate from the CANDELS-EGS field in the Bouwens et al. (2015) selection to validate potential $z \geq 7$ galax-

ies (though such observations have fortuitously become available as a result of observations made from the z9-CANDELS follow-up program [Bouwens et al. 2016]).

The apparent magnitudes of the $z = 7.1-8.5$ galaxies identified as part of the current selection are much brighter than the typical galaxy at $z \sim 8$, as is evident in both the upper and lower panels in Figure 9. In fact, 3 of the sources from our current IRAC-red $[3.6] - [4.5] > 0.5$ selection appear to represent the brightest $z \gtrsim 7.5$ galaxies known in the entire CANDELS program and constitute 3 of the 4 $z \sim 8$ candidates shown in the lower panel of Figure 9. The only other especially bright $H_{160,AB} \sim 25.0$ $z \sim 8$ candidate shown in that lower panel is presented in the appendix (since it satisfies our $[3.6] - [4.5] > 0.5$ selection criteria using an independent set of photometry, i.e., Skelton et al. 2014).

Interestingly enough, all 4 of the brightest candidates shown in the lower panel of Figure 9 are located in the CANDELS EGS field, providing a dramatic example of how substantial field-to-field variations in the surface densities of bright sources might be (though we note that EGSY-2008523660 is likely gravitationally lensed). This seems to be just a chance occurrence, as none of these candidates is clearly in a similar redshift window. The probability that the 4 brightest $z \sim 8$ sources in the CANDELS program would be found in the same CANDELS field (even if one is gravitationally lensed) is $\sim 1\%$.¹⁴

¹⁴ There is only one source from our combined $z \sim 8$ selection with Bouwens et al. (2015) which would be potentially easier to select as a $z \sim 8$ galaxy over the CANDELS EGS field. It is presented in Appendix A. Its redshift is not well constrained (lying anywhere between $z \sim 7.1$ and 8.5), but it would be marginally easier to find over the CANDELS EGS field since the Bouwens et

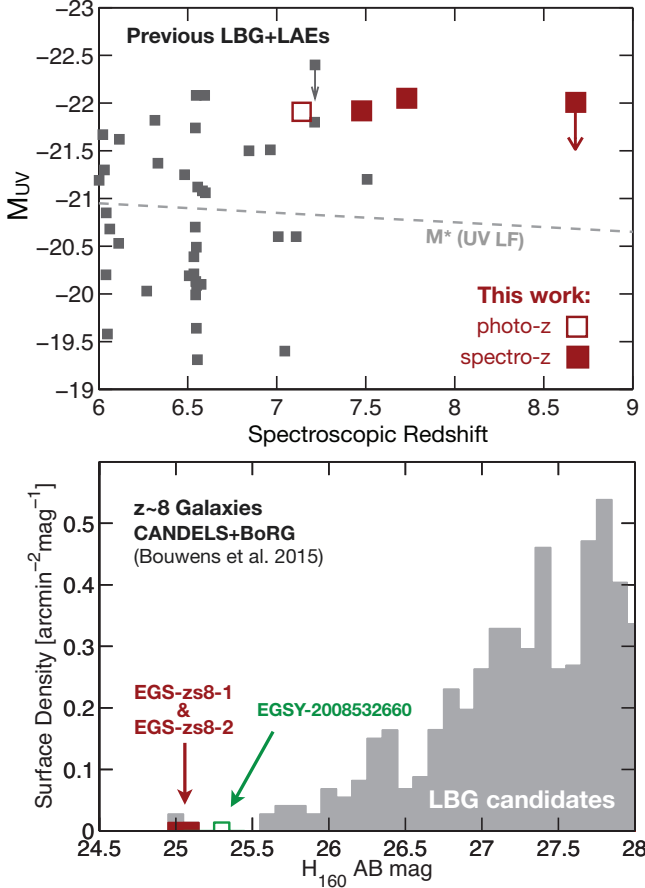


FIG. 9.— (*upper panel*) Absolute magnitudes vs. redshift in the rest-frame UV for sources in our current photometric sample (solid red squares for the two sources from our sample with redshift measurements from spectroscopy and open red squares where the redshift estimates derived from the photometry). For context, the absolute magnitudes and redshift measurements for other $z > 6$ galaxies in the literature with spectroscopic redshift measurements from Ly α are shown (black squares: compiled from Jiang et al. 2013, Finkelstein et al. 2013, Shibuya et al. 2012, Ono et al. 2012, and Vanzella et al. 2011). The gray-dashed line shows the evolution of the characteristic magnitude M^*_{UV} of the UV LF (Bouwens et al. 2015). Two sources from our sample, with redshift measurements from spectroscopy (the 4.7σ one requires further confirmation) are the brightest $z \gtrsim 7.5$ galaxies discovered at such high redshifts and similarly for our bright photometric $z \sim 8.6$ candidate (the downward arrow indicates the likely lensing magnification for this candidate: §3.4). (*lower panel*) Surface density of the full sample of $z \sim 8$ galaxies in the combined CANDELS and BoRG/HIPPIES fields (Bouwens et al. 2015, gray histogram). The shaded red squares indicate the position of our EGS-zs8-1 and EGS-zs8-2 in the Bouwens et al. (2015) $z \sim 8$ selections, while the open green square indicates the position of the $z \sim 8.6$ candidate EGSY-2008532660 (not identified as part of the Bouwens et al. 2015 $z \sim 8$ selection). Three of the sources from our selection represent the brightest-known galaxies at $z \gtrsim 7.5$ (although one appears to be magnified from gravitational lensing). Interestingly enough, all three of the brightest, highest-redshift $z \sim 8$ candidates we have identified here (and four if one includes the source from Appendix A which is also in the Bouwens et al. 2015 $z \sim 8$ catalog) are located in only one of the CANDELS fields (CANDELS EGS), providing an example of how dramatic field-to-field variance can be for bright galaxies (see also Bouwens et al. 2015 and Bowler et al. 2015).

al. (2015) $z \sim 8$ sample extends down to $z \sim 7$ over that field while the Bouwens et al. (2015) $z \sim 8$ samples over the other fields only extend down to $z \sim 7.3$.

Previously, this point had been strongly made by Bouwens et al. (2015) in discussing the number of bright sources over the different CANDELS fields (Figure 14, Appendices E and F from Bouwens et al. 2015) and also quite strikingly by Bowler et al. (2015) in comparing the number of bright $z \sim 6$ galaxies over the UltraVISTA and UDS fields.

6. IMPLICATIONS FOR THE BRIGHT END OF THE $z \sim 8$ LF

In this section, we will examine the implications of our present search results for the volume density of luminous galaxies in the $z \sim 7-9$ Universe. First, we estimate how complete we might expect our selection to be based on the $[3.6] - [4.5]$ color distribution in fields where the redshift can be constrained using deep Y -band data (§6.1). Second, we make use of our search results and our completeness estimates to set a constraint on the bright end of the $z \sim 7-9$ LF (§6.2).

6.1. $[3.6] - [4.5]$ Color Distribution of $z > 7$ Galaxies and the Implications for the Completeness of our red IRAC Criteria and the $[OIII] + H\beta$ EWs

In our attempts to identify bright $z > 7$ galaxies, we only consider those sources with red $[3.6] - [4.5] > 0.5$ Spitzer/IRAC colors to ensure that the sources we select are robustly at $z > 7$ (see §3.2). However, by making this requirement, we potentially exclude those $z > 7$ galaxies which have bluer $[3.6] - [4.5]$ colors, either due to lower-EW $[OIII] + H\beta$ lines or simply as a result of noise in the photometry.

To determine how important this effect is, we look at the $[3.6] - [4.5]$ color distribution of galaxies which we can robustly place at a redshift $z > 7$ (where both lines in $[OIII]$ doublet fall in the $[4.5]$ band). The most relevant sources are those bright galaxies we can place at $z > 7$ based on the available HST+ground-based photometry and which include deep flux measurements at $1\mu m$. Such measurements are available for the CANDELS GOODS-S, GOODS-N, UDS, and COSMOS fields, and a small fraction of the CANDELS EGS field.

For our fiducial results here, we only consider selected sources from those fields brightward of $H_{160,AB} = 26$ and with redshift estimates greater than $z \gtrsim 7.5$. This is to ensure that we only include bona-fide $z = 7.1-9.1$ galaxies (where the $[OIII] + H\beta$ line in the $4.5\mu m$ band) in our selection. Photometric redshift errors often have an approximate size of $\Delta z \sim 0.3$ to this magnitude limit, and so to avoid $z < 7$ sources scattering into our selection, we kept our cuts fairly conservative.

The list of such sources at such bright magnitudes is still somewhat limited at present, with only the bright ~ 25.6 -mag galaxy in the CANDELS South from Yan et al. (2012) and Oesch et al. (2012), a bright 25.7-mag galaxy in the CANDELS COSMOS field from Bouwens et al. (2015), a bright ~ 25.5 mag source over the CANDELS GOODS-North field by Finkelstein et al. (2013), two bright sources over the CANDELS EGS field where Y_{105} -band photometry is available (EGS-zs8-1, EGS-zs8-2), and a third bright source over the CANDELS EGS field where the $J_{125} - H_{160}$ color allows us to place it at $z > 8$ (EGSY-2008532660).

Of these sources, five out of the six sources have $[3.6] - [4.5]$ colors in excess of 0.5, and therefore for sim-

TABLE 3
BRIGHTEST $z \gtrsim 7.5$ GALAXIES OVER THE CANDELS FIELDS AND ~ 200 ARCMIN² BoRG/HIPPIES AREA SEARCHED BY BOUWENS ET AL. (2015)

ID	R.A.	Dec	m_{AB}^a	z_{phot}^b	[3.6] – [4.5]	References*
EGS-zs8-1	14:20:34.89	53:00:15.35	25.03 \pm 0.05	7.9 \pm 0.4 ($z_{spec}=7.7302\pm0.0006$)	0.53 \pm 0.09	[1], [8]
EGS-zs8-2	14:20:12.09	53:00:26.97	25.12 \pm 0.05	7.6 \pm 0.3 ($z_{spec}=7.4770\pm0.0008$)	0.96 \pm 0.17	[1]
EGSY-2008532660 [†]	14:20:08.50	52:53:26.60	25.26 \pm 0.09 [‡]	8.57 $^{+0.22}_{-0.43}$ ($z_{spec}=8.683^{+0.001}_{-0.004}$)	0.76 \pm 0.14	
GNDY-6379018085	12:36:37.90	62:18:08.50	25.44 \pm 0.04	7.508 ^c	0.88 \pm 0.11	[6]
BORGY-9469443552	04:39:46.94	–52:43:55.20	25.56 \pm 0.20	8.29 $^{+0.34}_{-1.01}$	—	[1],[2],[3], [7]
GSDY-2499348180	03:32:49.93	–27:48:18.00	25.58 \pm 0.05	7.84 $^{+0.15}_{-0.29}$	0.08 \pm 0.09	[1],[3],[4],[5]
BORGY-6504943342	14:36:50.49	50:43:34.20	25.69 \pm 0.08	7.49 $^{+0.13}_{-3.17}$	—	[1]
COSY-0235624462	10:00:23.56	02:24:46.20	25.69 \pm 0.07	7.84 $^{+0.37}_{-0.18}$	0.88 \pm 0.61	[1]
BORGY-2463351294	22:02:46.33	18:51:29.40	25.78 \pm 0.15	7.93 $^{+0.59}_{-0.21}$	—	[1]
BORGY-2447150300	10:32:44.71	50:50:30.00	25.91 \pm 0.20	7.93 $^{+0.48}_{-0.19}$	—	[1]
BORGY-5550543040	07:55:55.05	30:43:04.00	25.98 \pm 0.21	7.66 $^{+0.82}_{-5.63}$	—	[1]
Median					0.82 $^{+0.07}_{-0.20}$	
Other Possible Bright $z > 7.5$ Galaxies over CANDELS (Appendix A)						
EGSY-9597563148	14:19:59.75	52:56:31.40	25.03 \pm 0.10	8.19	0.22 \pm 0.06	[1]

* References: [1] Bouwens et al. 2015, [2] Bradley et al. 2012, [3] McLure et al. 2013, [4] Yan et al. 2012, [5] Oesch et al. 2012, [6] Finkelstein et al. 2013, [7] Schmidt et al. 2014, [8] Oesch et al. 2015b.

^a The apparent magnitude of each source in the H_{160} band.

^b Maximum likelihood photometric redshift estimate from EAZY.

^c Spectroscopic redshift determination (Finkelstein et al. 2013). Finkelstein et al. (2013) report a [3.6] – [4.5] color of 0.98 \pm 0.14.

[†] Photometric redshift estimate is not based on deep Y-band imaging observations over candidate of red [3.6] – [4.5] color as derived from the Bouwens et al. (2015) photometry. Inclusion in this list is based upon a red [3.6] – [4.5] color as derived from the Skelton et al. (2014) photometry.

[‡] The flux of this source seems likely to be boosted by gravitational lensing (§3.4).

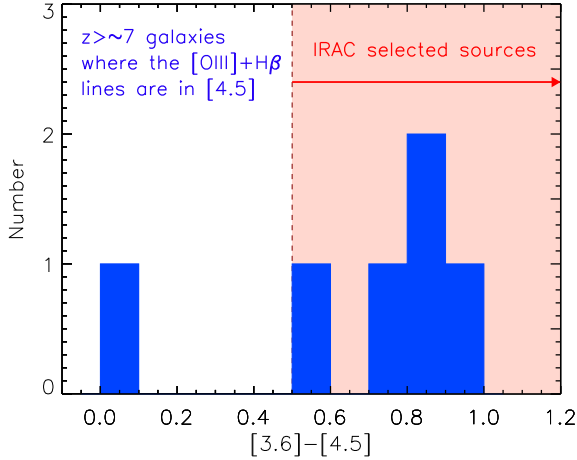


FIG. 10.— Range of Spitzer/IRAC [3.6] – [4.5] colors (blue histogram) observed for bright $z > 7$ galaxies where we are confident that the [OIII]+H β emission line falls in the [4.5] band (§6.1). Sources are included in this histogram if they are brighter than $H_{160,AB} = 26$ and the redshift information available on these sources confidently place them at $z \gtrsim 7.5$. This color distribution is compared against the IRAC red [3.6] – [4.5] > 0.5 selection criteria we use (shaded red region). The sources presented here are the same as those sources in Table 3 with IRAC color measurements. Five out of 6 $z \gtrsim 7.5$ galaxies show Spitzer/IRAC colors redder than 0.5. At face value, this suggests that our proposed [3.6] – [4.5] > 0.5 selection would identify 83 $^{+11}_{-16}$ % of the bright $z > 7$ population (but we emphasize this percentage is very uncertain due to the small numbers involved). The observed [3.6] – [4.5] color distribution also implies a minimum EW for [OIII]+H β of 1300Å.

plicity, we will assume that our IRAC red selection is 83% complete, but we emphasize that the completeness correction we derive from this selection is uncertain and could be much larger (as indeed one would expect if the [3.6] – [4.5] color measurement derived by Labbé et al. 2013, i.e., ~ 0.4 mag, for the average stacked $z \sim 8$ galaxy are indicative).

To investigate this possibility, we examined a slightly larger sample of objects over the four fields where we have photometric redshifts using Y-band imaging. Considering sources to a H_{160} -band magnitude limit of 26.2 over the CANDELS-UDS and COSMOS fields and 26.7 over the CANDELS GOODS-North and GOODS-South while extending the photometric redshift selection to $z > 7.3$, 6 out of 9 sources satisfy the [3.6] – [4.5] > 0.5 criterion. While this suggests the actual fraction of $z > 7$ galaxies with such red IRAC colors may be less than 83%, this fainter sample is still consistent with our fiducial percentage. It also reassuring that our suggested selection criteria would also apply to GN-108036, the bright $JH_{140} = 25.17$ $z = 7.213$ galaxy found by Ono et al. (2012), given its measured [3.6] – [4.5] color of 0.58 \pm 0.18 mag.

We include a list of those sources and other sources in Table 3 from the Bouwens et al. (2015) catalog and also including the bright $z = 7.508$ galaxy from Finkelstein et al. (2013). In Figure 10, we present the [3.6]–[4.5] color distribution for the brightest sources we know to robustly lie at $z \gtrsim 7.5$ based on spectroscopy or from the available HST+ground-based photometry for those sources that lie in regions of CANDELS with Y-band observations or with $J_{125} - H_{160}$ colors red enough to

confidently place the sources at $z > 8$.

The median $[3.6] - [4.5]$ color that we measure is $0.82^{+0.08}_{-0.20}$ mag. Such a color implies a minimum EW of $\sim 1300\text{\AA}$ for the $[\text{OIII}] + \text{H}\beta$ lines, assuming a flat stellar continuum and no line contribution to the $[3.6]$ band. However, we emphasize that if there is also a substantial line contribution to the $[3.6]$ band, e.g., from $\text{H}\gamma$, $\text{H}\delta$, and $[\text{OII}]$, then the implied EW of the $[\text{OIII}] + \text{H}\beta$ lines would be much larger. For example, adopting the line ratios from the Anders & Fritze-v. Alvensleben (2003), $0.2 Z_{\odot}$ model would imply an EW of $\gtrsim 2100\text{\AA}$ for the $[\text{OIII}] + \text{H}\beta$ lines.

Some correction is required to the median $[3.6] - [4.5]$ color measurement to account for the fact that the $z > 7$ sources from the CANDELS EGS field were explicitly selected because of their red IRAC colors. If we assume that the intrinsic $[3.6] - [4.5]$ color for sources over the CANDELS EGS field is ~ 0.6 mag (which is the value we find from the 3 candidates over the other CANDELS fields: see Table 3) and the noise + scatter is ~ 0.4 (the value from the other fields), we compute a bias of 0.24 mag from a simple Monte-Carlo simulation. Accounting for such biases reduces the median $[3.6] - [4.5]$ color of the population by 0.24 mag, which implies a median EW of $\sim 800\text{\AA}$ and 1500\AA , ignoring and accounting for a possible nebular contribution to the $[3.6]$ band respectively.

6.2. Volume Density of Bright $z \sim 8$ Galaxies

Here we use the search results from the previous section to set a constraint on the bright end of the $z \sim 8$ LF. We begin this section by calculating the total selection volume in which we would expect to find bright $z \geq 7$ galaxies with our selection criteria.

We will estimate the selection volumes in a similar way to the methodology used by Bouwens et al. (2015) in deriving the LFs from the full CANDELS program. In short, we create mock catalogs over each search field, with sources distributed over a range in both redshift $z \sim 6$ -10 and apparent magnitude ($H_{160,AB} = 24$ to 26). We then take the two-dimensional i_{775} -band images of similar luminosity, randomly-selected $z \sim 4$ galaxies from the HUDF (Bouwens et al. 2007, 2011, 2015) and create mock images of the sources at higher-redshift using the two dimensional pixel-by-pixel $z \sim 4$ galaxies as a guide (see Bouwens et al. 1998, 2003), adopting random orientations relative to their orientation in the HUDF and scaling their physical sizes as $(1+z)^{-1.2}$, which is the approximate relationship that has been found comparing the mean size of galaxies at fixed luminosity, as a function of redshift (Oesch et al. 2010; Grazian et al. 2012; Ono et al. 2013; Holwerda et al. 2015; Kawamata et al. 2015; Shibuya et al. 2015). Individual sources were assigned UV colors based on their UV luminosity, using the β - M_{UV} relationship derived by Bouwens et al. (2014) and allowing for an intrinsic scatter σ_{β} of 0.35 at high luminosities ($M_{UV,AB} = [-22, -20]$) as found by Bouwens et al. (2009, 2012) and systematically decreasing to 0.15 at lower luminosities as found by Rogers et al. (2014).

In addition to the HST images we created for individual sources, we also constructed simulated ground-based and Spitzer/IRAC images for these sources which we added to the real ground-based + Spitzer/IRAC data. These simulated images were generated based on the

mock H_{160} -band images we constructed for individual sources and convolving by the H_{160} -to-IRAC, H_{160} -to-ground kernels that MOPHONGO (Labbé et al. 2010) derived from the observations. In producing simulated IRAC images for the mock sources, we assume a rest-frame EW of 300\AA for $\text{H}\alpha + [\text{NII}]$ emission and 500\AA for $[\text{OIII}] + \text{H}\beta$ emission over the entire range $z = 4$ -9, a flat rest-frame optical color, and a H_{160} -optical continuum color of 0.2 - 0.3 mag, to match the observational results of Shim et al. (2011), Stark et al. (2013), González et al. (2012, 2014), Labbé et al. (2013), Smit et al. (2014, 2015), and Oesch et al. (2013).

We took the simulated images we created for individual sources and added them to the real HST, ground-based, and Spitzer/IRAC observations. These simulated images were, in turn, used to construct catalogs and our selection criteria applied to the derived catalogs in exactly the same way as we applied these criteria to the real observations (including excluding sources which violated our confusion criteria).

Summing the results over all five CANDELS fields, we compute a total selection volume of $1.6 \times 10^6 \text{ Mpc}^3$ per 1-mag interval for galaxies with $H_{160,AB}$ magnitudes brightward of 25.5 . If we assume that the present selection of $z \sim 8$ galaxies is complete, this would imply a volume density of $< 1.4 \times 10^{-6} \text{ Mpc}^{-3} \text{ mag}^{-1}$ and $3.8^{+3.7}_{-2.1} \times 10^{-6} \text{ Mpc}^{-3} \text{ mag}^{-1}$ for $H_{160,AB} \sim 24.5$ - 25.0 and $H_{160,AB} \sim 25.0$ - 25.5 galaxies, respectively. We ignore the contribution of the $z \sim 8.6$ candidate galaxy EGSY-2008532660, given the evidence that it may be slightly magnified (§3.4).

However, we cannot assume that the present selection of bright $z \sim 8$ galaxies is complete, since not every $z \sim 8$ galaxy exhibits such a red $[3.6] - [4.5]$ color. In the previous section, we found that only 5 out of the 6 bright ($H_{160,AB} < 26$), secure $z \gtrsim 7$ sources within CANDELS showed such red galaxies. Correcting the volume densities given in the previous paragraph to account for this slight empirically-derived incompleteness ($0.83^{+0.11}_{-0.16}$), we estimate volume densities of $< 1.7 \times 10^{-6} \text{ Mpc}^{-3} \text{ mag}^{-1}$ and $4.7^{+4.6}_{-2.7} \times 10^{-6} \text{ Mpc}^{-3} \text{ mag}^{-1}$ for $H_{160,AB} \sim 24.5$ - 25.0 and $H_{160,AB} \sim 25.0$ - 25.5 galaxies, respectively. The uncertainty in the completeness estimate is included in the error we quote for the volume density.

It is interesting to compare these constraints on the volume density of bright $z \sim 7.1$ - 8.5 galaxies with other recent constraints which are available on the volume density of bright end of the UV LFs at $z \sim 4$, $z \sim 6$, $z \sim 8$, and $z \sim 10$ galaxies from state-of-the-art studies (e.g., Bouwens et al. 2015). The results are shown in Figure 11, and it is clear that our result lies somewhere midway between the $z \sim 7$ and $z \sim 8$ LFs, as one might expect given the redshift distribution of the sources that make up our $z = 7.1$ - 8.5 sample.

7. SUMMARY

In this paper, we take advantage of the deep Spitzer/IRAC observations available over all five CANDELS in conjunction with the HST+ground-based data to conduct a search over 900 arcmin^2 to find bright $z \sim 8$ galaxies. To identify galaxies at such high redshifts, we select those galaxies with especially red Spitzer/IRAC $[3.6] - [4.5]$ colors (i.e., > 0.5), in the hopes of identifying

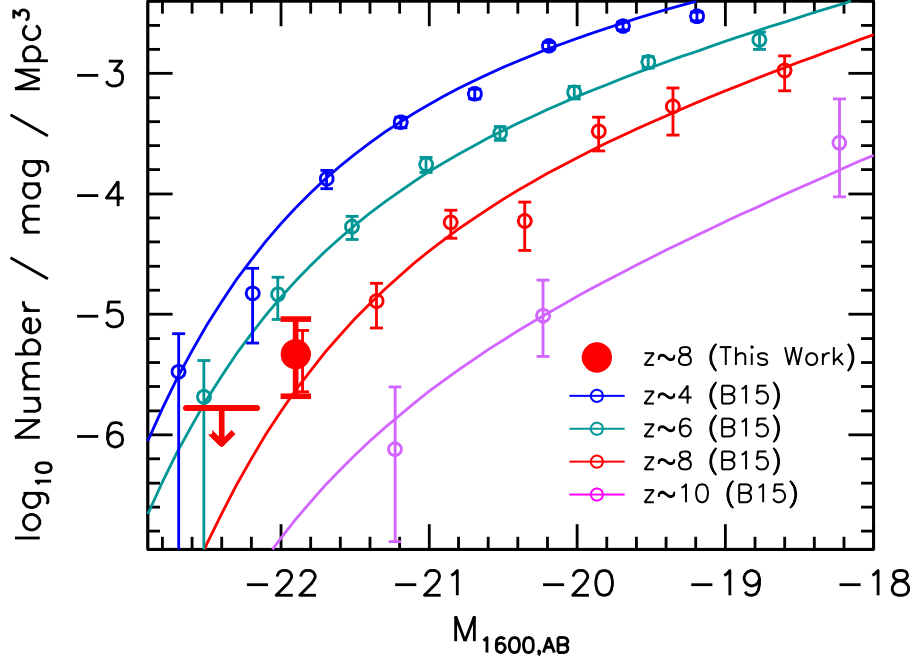


FIG. 11.— Estimated volume density of especially luminous $z \sim 7.1\text{--}9.1$ galaxies using the current IRAC-red search results over the entire CANDELS program (§6.2). This selection is assumed to be $17^{+16}_{-11}\%$ incomplete based on the results from §6.1 and excludes the $z \sim 8.6$ candidate galaxy EGSY-2008532660 due to evidence that this galaxy may be magnified by a foreground source (§3.4). For context, the UV luminosity function results of Bouwens et al. (2015: B15) at $z \sim 4$, $z \sim 6$, $z \sim 8$, and $z \sim 10$ are also shown with the blue, cyan, red, and magenta open circles and solid lines, respectively. The present constraints on the UV LF are consistent with those previously derived by Bouwens et al. (2015).

those $z \gtrsim 6$ galaxies which show the presence of a strong $[\text{OIII}]+\text{H}\beta$ line in $4.5\mu\text{m}$ band. Such a selection is useful for the CANDELS program, given the lack of uniformly deep Y -band observations over all five fields.

Our selection yielded 4 $z \geq 7$ candidates brighter than an $H_{160,AB}$ magnitude of 25.5. Each of these four selected candidates was required to be undetected ($<2.5\sigma$) at optical wavelengths ($<1\mu\text{m}$), as defined by the inverse-variance-weighted mean flux measurement, be undetected in the V_{606} -band ($<1.5\sigma$), and show a $I_{814} - J_{125}$ color redward of 1.5.

Fortuitously, 3 of our 4 selected $z \geq 7$ candidates had deep Y -band observations available from either deep ground-based observations or from the new z9-CANDELS follow-up program (Bouwens 2014; Bouwens et al. 2016) with HST. The available Y -band observations provide clear confirmation of the $z \geq 7$ redshifts we estimate for three of four candidates found in our search.

The redshift estimates we obtain for three of our selected candidates lie significantly above $z \sim 7$, with EGS-zs8-2 having a redshift estimate of 7.6 ± 0.3 , EGS-zs8-1 having a redshift estimate of 7.9 ± 0.4 , and EGSY-2008532660 having a redshift estimate of $8.6^{+0.2}_{-0.4}$.

We also obtained spectroscopic observations on two of our candidate $z > 7$ galaxies in the near-IR and find probable $\text{Ly}\alpha$ lines in their spectra consistent with redshifts of 7.4770 ± 0.0008 and 7.7302 ± 0.0006 . The detection of $\text{Ly}\alpha$ emission for these candidates is significant at 4.7σ and 6.1σ significance, respectively. The second of these sources was featured in Oesch et al. (2015b). Remarkably enough, a third candidate from our list was spectroscopically confirmed to lie at $z = 8.683$ by Zitrin

et al. (2015).

These sources represent the brightest $z \geq 7.5$ candidates we identified over the entire CANDELS program and are 0.5-mag brighter than $z \geq 7.5$ candidates identified anywhere else on the sky. Coincidentally enough, they all lie in the same CANDELS field, again suggesting large field-to-field variations for brightest $z \geq 7$ galaxies. See also discussion in Bouwens et al. (2015) and Bowler et al. (2015).

Using these candidates, we estimate the volume density of bright ($H_{160,AB} < 25.5$) $z \geq 7$ galaxies in the early Universe based on our selected sample and estimate that $17^{+16}_{-11}\%$ of $z > 7$ galaxies do not show such red colors. The volume density estimate we derive lies midway between the volume density of luminous $z \sim 6$ galaxies Bouwens et al. (2015) derive and the volume density of luminous $z \sim 8$ galaxies.

The median $[3.6] - [4.5]$ color distribution for our selection and other bright $z \gtrsim 7.5$ galaxies from the literature is $0.82^{+0.08}_{-0.20}$ mag (observed) and $0.58^{+0.08}_{-0.20}$ (correcting for the approximate selection bias: see §6.1). This strongly points to the existence of extremely high EW nebular emission lines in typical star-forming galaxies at $z > 7$. Assuming no contribution from nebular line emission to the $[3.6]$ band implies a $[\text{OIII}]+\text{H}\beta$ EW of $\sim 800\text{\AA}$. However, allowing for contamination of the $[3.6]$ band in accordance with the expectations of Anders & Fritze-v. Alvensleben (2003) would imply a median EW of $\sim 1500\text{\AA}$. These results are in reasonable agreement but perhaps slightly higher than Smit et al. (2015) estimate for the IRAC-blue sources they selected at $z = 6.6\text{--}6.9$. Smit et al. (2015) estimate a typical $[\text{OIII}] + \text{H}\beta$ EW of 1085\AA

for their selected sources. These estimates are similar albeit slightly higher than those estimated by Labbé et al. (2013), Laporte et al. (2014, 2015), and Huang et al. (2016).

In the near future, we would expect the brightest $z \sim 8$ galaxies to be identified within the $\sim 1 \text{ deg}^2$ wide-area UltraVISTA field (McCracken et al. 2012) by combining the progressively deeper $YJHK_s$ observations with constraints from the optical Subaru+CFHT observations and Spitzer/IRAC observations from SPLASH (Capak et al. 2013) and SMUVS (Caputi et al. 2014). Another significant source of bright $z \sim 8$ candidates will be the new BoRG_[z910] program (Trenti 2014), which uses a huge allotment of 500 orbits to cover a 500 arcmin^2 area to

$\gtrsim 26.5 \text{ mag}$ depth (5σ).

We thank Robert Barone-Nugent, Daniel Schaerer and Dan Stark for valuable conversations. This work has benefited significantly from the public reductions of the SEDS program and hence the efforts of Matt Ashby, Giovanni Fazio, Steve Willner, and Jiasheng Huang. We are grateful to Dan Stark, Sirio Belli, and Richard Ellis for communicating with us with some unpublished results they also obtained on EGS-zs8-2 (April 2015) where they also find a $>3\sigma$ line (putatively Ly α) at $1.031 \mu\text{m}$ (to appear in D. Stark et al. 2016, in prep). We acknowledge the support of NASA grant NAG5-7697, NASA grant HST-GO-11563, and a NWO vrij competitie grant 600.065.140.11N211.

REFERENCES

- Anders, P., & Fritze-v. Alvensleben, U. 2003, *A&A*, 401, 1063
 Ashby, M. L. N., Willner, S. P., Fazio, G. G., et al. 2013, *ApJ*, 769, 80
 Atek, H., Richard, J., Jauzac, M., et al. 2015, *ApJ*, 814, 69
 Barone-Nugent, R. L., Wyithe, J. S. B., Trenti, M., et al. 2015, *MNRAS*, 450, 1224
 Bertin, E., & Arnouts, S. 1996, *A&AS*, 117, 393
 Bouwens, R., Broadhurst, T. and Silk, J. 1998, *ApJ*, 506, 557
 Bouwens, R. J., Illingworth, G. D., Rosati, P., et al. 2003, *ApJ*, 595, 589
 Bouwens, R. J., Illingworth, G. D., Franx, M., & Ford, H. 2007, *ApJ*, 670, 928
 Bouwens, R. J., Illingworth, G. D., Oesch, P. A., et al. 2011, *ApJ*, 737, 90
 Bouwens, R. J., Illingworth, G. D., Oesch, P. A., et al. 2012, *ApJ*, 754, 83
 Bouwens, R. 2014, HST Proposal, 13792
 Bouwens, R. J., Illingworth, G. D., Oesch, P. A., et al. 2015, *ApJ*, 803, 34
 Bouwens, R. J., Oesch, P. A., Labbe, I., et al. 2016, submitted, arXiv:1506.01035
 Bowler, R. A. A., Dunlop, J. S., McLure, R. J., et al. 2014, *MNRAS*, 440, 2810
 Bowler, R. A. A., Dunlop, J. S., McLure, R. J., et al. 2015, *MNRAS*, 452, 1817
 Burgasser, A. J., McElwain, M. W., Kirkpatrick, J. D., et al. 2004, *AJ*, 127, 2856
 Bradley, L. D., Bouwens, R. J., Ford, H. C., et al. 2008, *ApJ*, 678, 647
 Bradley, L. D., Trenti, M., Oesch, P. A., et al. 2012, *ApJ*, 760, 108
 Bradley, L. D., Zitrin, A., Coe, D., et al. 2014, *ApJ*, 792, 76
 Brammer, G. B., van Dokkum, P. G., & Coppi, P. 2008, *ApJ*, 686, 1503
 Capak, P., Aussel, H., Ajiki, M., et al. 2007, *ApJS*, 172, 99
 Capak, P., Aussel, H., Bundy, K., et al. 2013, Spitzer Proposal, 10042
 Caputi, K., Ashby, M., Fazio, G., et al. 2014, Spitzer Proposal, 11016
 de Barros, S., Schaerer, D., & Stark, D. P. 2014, *A&A*, 563, A81
 Ellis, R. S., McLure, R. J., Dunlop, J. S., et al. 2013, *ApJ*, 763, LL7
 Fialkov, A., & Loeb, A. 2015, *ApJ*, 806, 256
 Finkelstein, S. L., Papovich, C., Dickinson, M., et al. 2013, *Nature*, 502, 524
 Finkelstein, S. L., Ryan, R. E., Jr., Papovich, C., et al. 2014, ArXiv e-prints
 Furusawa, H., Kosugi, G., Akiyama, M., et al. 2008, *ApJS*, 176, 1
 Fontana, A., Dunlop, J. S., Paris, D., et al. 2014, *A&A*, 570, AA11
 Galametz, A., Grazian, A., Fontana, A., et al. 2013, *ApJS*, 206, 10
 González, V., Bouwens, R. J., Labbé, I., et al. 2012, *ApJ*, 755, 148
 González, V., Bouwens, R., Illingworth, G., et al. 2014, *ApJ*, 781, 34
 Grazian, A., Castellano, M., Fontana, A., et al. 2012, *A&A*, 547, A51
 Grogan, N. A., Kocevski, D. D., Faber, S. M., et al. 2011, *ApJS*, 197, 35
 Guo, Y., Ferguson, H. C., Giavalisco, M., et al. 2013, *ApJS*, 207, 24
 Holwerda, B. W., Bouwens, R., Oesch, P., et al. 2015, *ApJ*, 808, 6
 Huang, K.-H., Bradač, M., Lemaux, B. C., et al. 2016, *ApJ*, 817, 11
 Ishigaki, M., Kawamata, R., Ouchi, M., et al. 2015, *ApJ*, 799, 12
 Jiang, L., Egami, E., Mechtley, M., et al. 2013, *ApJ*, 772, 99
 Kawamata, R., Ishigaki, M., Shimasaku, K., Oguri, M., & Ouchi, M. 2015, *ApJ*, 804, 103
 Kirkpatrick, J. D., Cushing, M. C., Gelino, C. R., et al. 2011, *ApJS*, 197, 19
 Koekemoer, A. M., Faber, S. M., Ferguson, H. C., et al. 2011, *ApJS*, 197, 36
 Kotulla, R., Fritze, U., Weilbacher, P., & Anders, P. 2009, *MNRAS*, 396, 462
 Kriek, M., Shapley, A. E., Reddy, N. A., et al. 2015, *ApJS*, 218, 15
 Kron, R. G. 1980, *ApJS*, 43, 305
 Labbé, I., et al. 2010a, *ApJ*, 708, L26
 Labbé, I., et al. 2010b, *ApJ*, 716, L103
 Labbé, I., Oesch, P. A., Bouwens, R. J., et al. 2013, *ApJ*, 777, LL19
 Labbé, I., Oesch, P. A., Illingworth, G. D., et al. 2015, *ApJS*, 221, 23
 Laporte, N., Streblyanska, A., Clement, B., et al. 2014, *A&A*, 562, L8
 Laporte, N., Streblyanska, A., Kim, S., et al. 2015, *A&A*, 575, A92
 Lorenzoni, S., Bunker, A. J., Wilkins, S. M., et al. 2013, *MNRAS*, 429, 150
 Mason, C. A., Treu, T., Schmidt, K. B., et al. 2015, *ApJ*, 805, 79
 McLean, I. S., Steidel, C. C., Epps, H. W., et al. 2012, *Proc. SPIE*, 8446, 84460J
 McCracken, H. J., Milvang-Jensen, B., Dunlop, J., et al. 2012, *A&A*, 544, A156
 McLeod, D. J., McLure, R. J., Dunlop, J. S., et al. 2015, *MNRAS*, 450, 3032
 McLure, R. J., Dunlop, J. S., Bowler, R. A. A., et al. 2013, *MNRAS*, 432, 2696
 Oesch, P. A., et al. 2010a, *ApJ*, 709, L16
 Oesch, P. A., Bouwens, R. J., Illingworth, G. D., et al. 2012, *ApJ*, 759, 135
 Oesch, P. A., Labbé, I., Bouwens, R. J., et al. 2013, *ApJ*, 772, 136
 Oesch, P. A., Bouwens, R. J., Illingworth, G. D., et al. 2014, *ApJ*, 786, 108
 Oesch, P. A., Bouwens, R. J., Illingworth, G. D., et al. 2015a, *ApJ*, 808, 104
 Oesch, P. A., van Dokkum, P. G., Illingworth, G. D., et al. 2015b, *ApJ*, 804, L30
 Oke, J. B., & Gunn, J. E. 1983, *ApJ*, 266, 713
 Ono, Y., Ouchi, M., Mobasher, B., et al. 2012, *ApJ*, 744, 83
 Ono, Y., Ouchi, M., Curtis-Lake, E., et al. 2013, *ApJ*, 777, 155
 Pentericci, L., Fontana, A., Vanzella, E., et al. 2011, *ApJ*, 743, 132

- Rogers, A. B., McLure, R. J., Dunlop, J. S., et al. 2014, *MNRAS*, 440, 3714
- Schaerer, D., & de Barros, S. 2009, *A&A*, 502, 423
- Schenker, M. A., Stark, D. P., Ellis, R. S., et al. 2012, *ApJ*, 744, 179
- Schenker, M. A., Robertson, B. E., Ellis, R. S., et al. 2013, *ApJ*, 768, 196
- Schmidt, K. B., Treu, T., Trenti, M., et al. 2014, *ApJ*, 786, 57
- Shibuya, T., Kashikawa, N., Ota, K., et al. 2012, *ApJ*, 752, 114
- Shibuya, T., Ouchi, M., & Harikane, Y. 2015, *ApJS*, 219, 15
- Shim, H., Chary, R.-R., Dickinson, M., et al. 2011, *ApJ*, 738, 69
- Skelton, R. E., Whitaker, K. E., Momcheva, I. G., et al. 2014, *ApJS*, 214, 24
- Smit, R., Bouwens, R. J., Labbé, I., et al. 2014, *ApJ*, 784, 58
- Smit, R., Bouwens, R. J., Franx, M., et al. 2015, *ApJ*, 801, 122
- Stark, D. P., Schenker, M. A., Ellis, R., et al. 2013, *ApJ*, 763, 129
- Szalay, A. S., Connolly, A. J., & Szokoly, G. P. 1999, *AJ*, 117, 68
- Tilvi, V., Papovich, C., Tran, K.-V. H., et al. 2013, *ApJ*, 768, 56
- Trenti, M., Bradley, L. D., Stiavelli, M., et al. 2011, *ApJ*, 727, L39
- Treu, T., Schmidt, K. B., Trenti, M., Bradley, L. D., & Stiavelli, M. 2013, *ApJ*, 775, LL29
- Trenti, M. 2014, HST Proposal, 13767
- Vanzella, E., Pentericci, L., Fontana, A., et al. 2011, *ApJ*, 730, L35
- Wilkins, S. M., Coulton, W., Caruana, J., et al. 2013, *MNRAS*, 435, 2885
- Wilkins, S. M., Stanway, E. R., & Bremer, M. N. 2014, *MNRAS*, 439, 1038
- Windhorst, R. A., Cohen, S. H., Hathi, N. P., et al. 2011, *ApJS*, 193, 27
- Wyithe, J. S. B., Yan, H., Windhorst, R. A., & Mao, S. 2011, *Nature*, 469, 181
- Yan, H., Yan, L., Zamojski, M. A., et al. 2011, *ApJ*, 728, LL22
- Yan, H., Finkelstein, S. L., Huang, K.-H., et al. 2012, *ApJ*, 761, 177
- Zheng, W., Postman, M., Zitrin, A., et al. 2012, *Nature*, 489, 406 (Z12)
- Zheng, W., Shu, X., Moustakas, J., et al. 2014, *ApJ*, 795, 93
- Zitrin, A., Zheng, W., Broadhurst, T., et al. 2014, *ApJ*, 793, L12

TABLE 4
ADDITIONAL BRIGHT ($H_{160,AB} < 25.5$) $z \geq 7$ SOURCE IDENTIFIED OVER THE CANDELS FIELDS
UTILIZING THE SKELTON ET AL. (2014) CATALOGS FOR SOURCE SELECTION.

ID	R.A.	Dec	m_{AB}^a	$[3.6] - [4.5]$	z_{phot}^b	References [*]
EGSY-9597563148	14:19:59.76	52:56:31.40	25.03 ± 0.10	0.53 ± 0.26^c	$8.19^{+0.23}_{-0.87}$	[1]
component-a	14:19:59.78	52:36:31.30	25.73 ± 0.14			
component-b	14:19:59.73	52:36:31.70	25.83 ± 0.13			

^{*} References: [1] Bouwens et al. 2015

^a The apparent magnitude of each source in the H_{160} band.

^b Maximum likelihood photometric redshift estimate from EAZY.

^c This is the $[3.6] - [4.5]$ color that Skelton et al. (2014) measure. Since our selection use the Spitzer/IRAC photometry from Bouwens et al. (2015) when available and Bouwens et al. (2015) measure a $[3.6] - [4.5]$ color of ~ 0.2 for the source, we do not include this source in our primary selection.

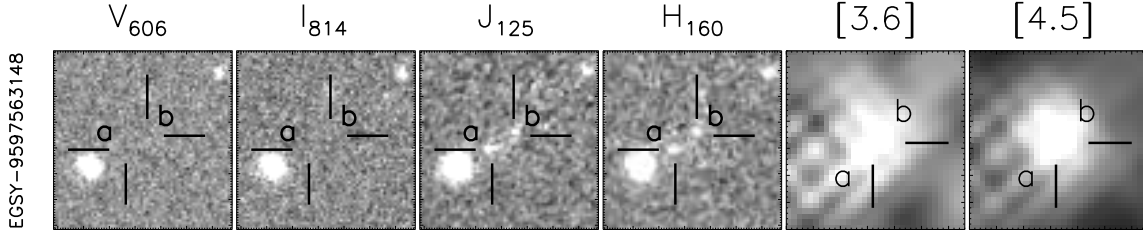


FIG. 12.— HST/ACS $V_{606}I_{814}$ and HST/WFC3 $J_{125}H_{160}$ postage stamp cut-outs ($4'' \times 4''$) of one particularly bright ($H_{160,AB} < 25.5$) $z \geq 7$ galaxy candidate selected by applying our IRAC-red criteria ($[3.6] - [4.5] > 0.5$) to the Skelton et al. (2014) photometric catalog. This source also has a red $[3.6] - [4.5]$ color in the Bouwens et al. (2015) catalog, but do not quite satisfy our IRAC-red selection criterion. This galaxy appears to consist of two separate components (indicated with black hash marks and the labels “a” and “b” respectively). The photometry for each component is provided in Table 4.

APPENDIX

A. OTHER CANDIDATE $z \geq 7$ GALAXIES

In addition to our application of our criteria to the catalogs Bouwens et al. (2015) compiled over a 750 arcmin^2 search area within CANDELS, we also made use of the catalogs from the 3D-HST team (Skelton et al. 2014) over the same region. Our rationale to do so was to maximize the completeness of our selection for bright $z \geq 7$ galaxies.

One additional $z \geq 7$ galaxy candidate is found which did not make it into our fiducial selection using the Bouwens et al. (2015) catalogs (because it had a measured $[3.6] - [4.5]$ color of $\sim 0.2 \text{ mag}$).¹⁵ We tabulate its coordinates, $H_{160,AB}$ -band magnitude, $[3.6] - [4.5]$ color, and estimated redshift in Table 4. Postage images of the $z \sim 8$ candidate is presented in Figure 12. Model fits to the photometry Skelton et al. (2014) provide on the source, as well as the inferred redshift likelihood distribution, are also presented in Figure 13.

B. SOURCES USED TO VALIDATE OUR PROPOSED $[3.6] - [4.5] > 0.5$ SELECTION

In §3.2, we considered a selection of sources from the four CANDELS fields with deep Y -band observations to test the idea that we could use an IRAC color criterion, i.e., $[3.6] - [4.5] > 0.5$, combined with an optical dropout criterion to identify galaxies at $z > 7$ even in the absence of Y -band data.

In Table 5, we provide a compilation of the 15 sources that we identified which satisfied the primary selection criteria from the paper but which are brighter than 26.7 mag in the H_{160} -band (and brighter than 26.5 mag over the CANDELS UDS and COSMOS fields).

¹⁵ While such differences might seem to be a concern, the $[3.6] - [4.5]$ colors we measure for the 4 other sources in our se-

lection agree to $< 0.1 \text{ mag}$ with the Skelton et al. (2014) values ($\sim 0.05 \text{ mag}$ differences are typical).

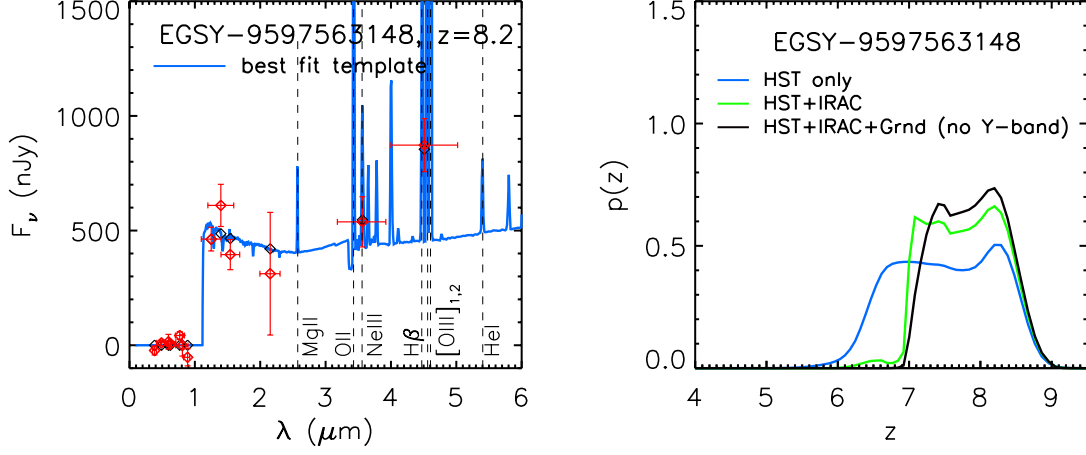


FIG. 13.— *Left:* Best-fit SED models (*blue line*) to the observed HST + Spitzer/IRAC + ground-based photometry (*red points and error bars*) for one especially bright ($H_{160,AB} < 25.5$) $z \geq 7$ galaxies identified by applying our IRAC-red selection criteria ($[3.6] - [4.5] > 0.5$) to the Skelton et al. (2014) photometric samples. *Right:* The redshift likelihood distribution $P(z)$ for the same candidate $z \geq 7$ galaxy, as computed by EAZY using the Skelton et al. (2014) photometry.

TABLE 5
SOURCES IN THE 4 CANDELS FIELDS WITH DEEP Y-BAND DATA USED TO
VALIDATE OUR PROPOSED SELECTION TECHNIQUE (§3.2)

ID [†]	R.A.	Dec	$m_{160,AB}$	$[3.6] - [4.5]$	z_{phot}^{\ddagger}
GNDY-6487514332	12:36:48.752	62:14:33.29	26.4	$0.6^{+0.7}_{-0.6}$	7.66
GNDY-7048017191	12:37:04.805	62:17:19.14	26.2	$1.1^{+0.3}_{-0.2}$	7.84
GNWY-7379420231	12:37:37.941	62:20:23.14	26.5	$0.5^{+1.5}_{-0.5}$	8.29
GNWZ-7455218088	12:37:45.529	62:18:08.87	26.5	$0.7^{+0.2}_{-0.2}$	7.16
GSDZ-2468850074	03:32:46.889	-27:50:07.45	26.0	$1.1^{+0.1}_{-0.1}$	7.24
GSWY-2249353259	03:32:24.934	-27:53:25.94	26.1	$0.6^{+0.2}_{-0.3}$	8.11
GSDY-2209651370	03:32:20.964	-27:51:37.02	26.3	$1.0^{+1.8}_{-0.8}$	7.84
COSY-0439027359	10:00:43.90	2:27:35.9	26.6	$0.7^{+0.2}_{-0.2}$	7.33
COSZ-0237620370*	10:00:23.76	2:20:37.0	25.1	$1.0^{+0.2}_{-0.1}$	7.14
COSY-0235624462	10:00:23.56	2:24:46.2	25.7	$0.9^{+0.1}_{-0.1}$	7.84
UDSY-4133353345	02:17:41.333	-5:15:33.45	25.8	$0.5^{+0.2}_{-0.2}$	7.41
UDSY-4308785165	02:17:43.087	-5:08:51.65	26.3	$0.7^{+0.8}_{-0.5}$	7.84
UDSZ-419355469	02:17:41.993	-5:15:54.69	26.5	$1.8^{+2.6}_{-0.6}$	7.08
UDSY-1765825082	02:17:17.658	-5:12:50.82	26.3	$1.1^{+0.1}_{-0.1}$	7.93
UDSY-5428621201	02:16:54.286	-5:12:12.01	26.1	$1.0^{+1.1}_{-0.7}$	7.49

* Also featured in our primary selection.

[†] IDs are from the Bouwens et al. (2015) catalog.

[‡] Photometric redshift computed based on the HST and deep ground-based data (i.e., not including constraints from the IRAC data).